ALMA MATER STUDIORUM - UNIVERSITÀ DI BOLOGNA

SCUOLA DI INGEGNERIA E ARCHITETTURA

DIPARTIMENTO DI INGEGNERIA INDUSTRIALE - DIN

CORSO DI LAUREA MAGISTRALE IN INGEGNERIA MECCANICA

TESI DI LAUREA

in

Meccanica delle Macchine M

PERFORMANCE ANALYSIS OF CABLE-DRIVEN WRENCH APPLICATORS

CANDIDATO:
Federico Guerra

RELATORE:
Prof. Ing. Marco Carricato

CORRELATORI:
Ing. Edoardo Idà
Prof. Ing. Sunil Agrawal

Anno accademico 2023/2024

Sessione V

To Eliza, with gratitude for your endless support throughout this journey.

To Cinzia, Michele, and Cecilia, for always believing in me.

Abstract

Cable-Driven Wrench Applicators (CDWA) are robotic systems that use multiple cables to generate forces and moments (wrench) at the end-effector (EE). In many applications, only certain components of the wrench need to be precisely controlled, while the remaining components need to be managed according to some criteria. This thesis proposes a framework for analyzing and comparing CDWAs with an arbitrary number of cables greater than the number of wrench components to be controlled. The framework introduces three performance indices to (i) optimize the tension distribution across the cables, (ii) evaluate the tension on the cables, and (iii) analyze the quality of the applied wrench. It allows determining the minimum number of cables required, comparing different architectures, and supporting the design of new tasks. The effectiveness of the framework is demonstrated by comparing an 8-cable and a 4-cable system in a rehabilitation scenario. Simulations and experimental validation show that the 4-cable system, while requiring higher tensions, achieves comparable performance in terms of applied wrench, while offering greater ease of use and mechanical simplicity. These results suggest that task-specific optimization of cable robots can improve usability without compromising performance, providing relevant insights for the design and optimization of new CDWAs.

I Cable-Driven Wrench Applicators (CDWA) sono sistemi robotici che utilizzano più cavi per generare forze e momenti (wrench) sull'end-effector (EE). In molte applicazioni, solo alcune componenti del wrench devono essere controllate con precisione, mentre le restanti componenti devono essere gestite secondo alcuni criteri. Questa tesi propone un framework per analizzare e confrontare i CDWA con un numero arbitrario di cavi superiore al numero di componenti del wrench da controllare. Il framework introduce tre indici di performance per (i) ottimizzare la distribuzione delle tensioni sui cavi, (ii) valutare le tensioni sui cavi e (iii) analizzare la qualità del wrench applicato. Permette di determinare il numero minimo di cavi necessari, confrontare diverse architetture e supportare la progettazione di nuovi task. L'efficacia del framework è dimostrata attraverso il confronto tra un sistema a 8 cavi e uno a 4 cavi in un contesto di riabilitazione. Le simulazioni e la convalida sperimentale dimostrano che il sistema a 4 cavi, pur richiedendo tensioni più elevate, raggiunge prestazioni comparabili in termini di wrench applicato, offrendo al contempo una maggiore facilità d'uso e semplicità meccanica. Questi risultati suggeriscono che l'ottimizzazione specifica dei robot a cavi per un determinato task può migliorare l'usabilità senza compromettere le prestazioni, fornendo indicazioni rilevanti per la progettazione e l'ottimizzazione di nuovi CDWA.

Contents

Chapter 1

Introduction

1.1 Cable-Driven Parallel Robots for Precise Force Control

In many real-world robotic applications, it is essential to decouple the control of position from the ability to exert forces and moments (collectively referred to as *wrench*). This separation is particularly important in systems where the primary goal is to apply precise wrenches, while delegating positional control to an external mechanism or operator. Examples include rehabilitation devices [1], training simulators [2], and haptic interfaces [3], where precise force application is critical to achieving desired outcomes. Cable-driven parallel robots (CDPRs) are a class of robotic systems uniquely suited for such tasks, due to their inherent advantages related to force control [4]. Unlike traditional rigid-link robots, CDPRs use multiple cables to manipulate an end-effector within a workspace (Fig. 1.1). By adjusting the tension in these cables, CDPRs can apply controlled forces and moments to the end-effector with relatively high precision. These systems offer several advantages, including a larger and scalable workspace, simpler mechanical design, reduced inertia, and the ability to achieve precise force control with minimal complexity [5].

A specific subset of these systems, known as *cable-driven wrench applicators* (CDWAs), focuses exclusively on applying wrenches (forces and moments) without directly controlling the end-effector position. CDWAs offer several distinct advantages over traditional rigid-link robotic systems, as highlighted in [6]. First, their cable-driven design allows for adaptable and dynamic force application, enabling them to deliver forces in multiple directions with adjustable magnitudes. This flexibility is crucial for tasks such as gait training, postural control, and balance rehabilitation, where forces need to be tailored to the user's specific needs. Second, CDWAs modular design allows for scalability and customization, enabling the same system to be adapted for different users or applications. Third, the versatility offered by CDWAs makes them suitable for a broader range of applications compared to current rigid-link rehabilitation devices, enabling the rehabilitation of many additional body parts.

However, one of the most significant advantages of CDWAs that makes them inherently suitable for rehabilitation is their low inertia, which stems from the use of lightweight cables instead of rigid links [7]. Unlike rigid-link exoskeletons, which add substantial mass and inertia to the human body, CDWAs allow patients to move freely without the burden of additional weight. This is critical for simulating natural human movement during rehabilitation, as it ensures the therapy to not be biased by the me-

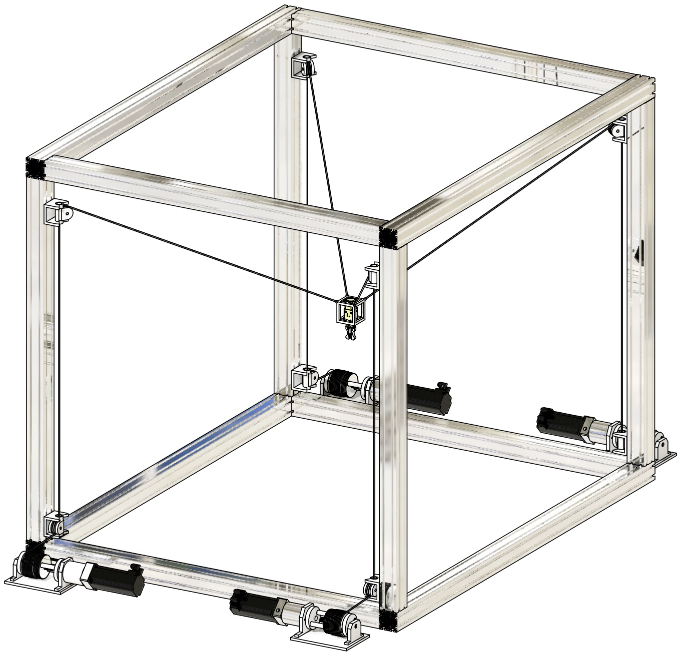

Figure 1.1: Example of a 4-cable *CDPR*

chanical properties of the device. For example, rigid-link exoskeletons can alter a patient's gait or posture due to their added mass and inertia, potentially leading to suboptimal therapeutic outcomes. In contrast, CDWAs provide precise force application while maintaining the natural dynamics of human motion, making them ideal for applications where movement quality and authenticity are crucial.

The ROAR Lab at Columbia University, with whom this work is in collaboration, has pioneered the development of CDWAs for rehabilitation purposes, creating innovative devices such as the Trunk Support Trainer (TruST, Fig.1.2a), Tethered Pelvic Assist Device (TPAD, Fig.1.2b), Robotic Upper-body Support Trainer (RobUST, Fig.1.3a), and Mobile Tethered Pelvic Assist Device (mTPAD, Fig.1.3b). These devices have been successfully applied in various rehabilitation tasks, including improving sitting postural control [8], enhancing standing ability in individuals with spinal cord injuries [9], promoting gait symmetry and weight-bearing in stroke survivors [10], and improving balance and cognitive performance in older adults [11]. Additionally, they have been used to measure and expand postural workspace during sitting in people with spinal cord injuries [12]. These advancements highlight the transformative potential of CDWAs in rehabilitation.

1.2 Challenges in Cable-Driven Wrench Applicators (CDWAs)

Cable-Driven Parallel Robots (CDPRs) have been extensively studied for their use as traditional position-controlled robots, with significant research focused on workspace analysis [13] and performance evaluation [14]. However, when these systems are repurposed primarily for wrench application, i.e. applying controlled forces and moments to an object or user, there is a notable lack of comprehensive frameworks for evaluating and optimizing their performance. This gap is particularly concerning given the growing demand for such systems across a wide range of applications, including

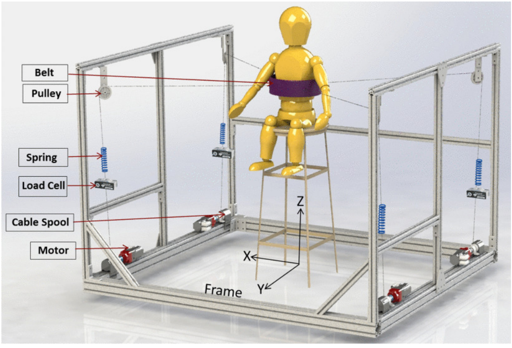

(a) TruST robot

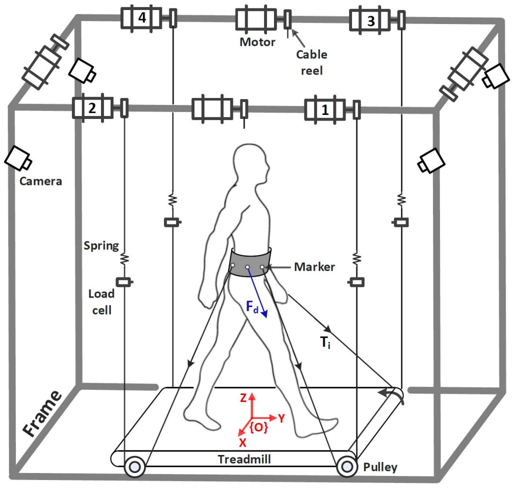

(b) TPAD robot

Figure 1.2: Example of two 4-cable driven wrench applicators for rehabilitation

(a) RobUST robot

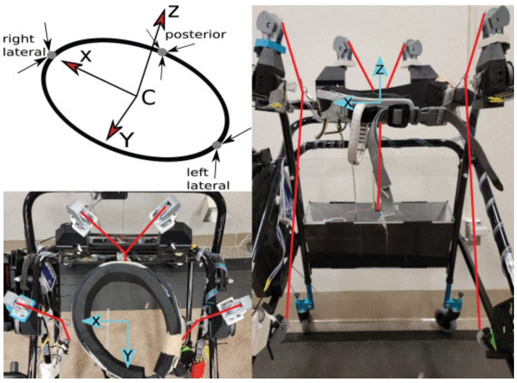

(b) mTPAD robot

Figure 1.3: Example of a 8- and a 6-cable driven wrench applicator for rehabilitation

rehabilitation, manufacturing, and aerospace.

The unique challenges of force-focused applications in CDPRs stem from their inherent design and operational characteristics. Unlike position-controlled robots, where the primary goal is to achieve precise movement, wrench applicators must prioritize the accurate and efficient delivery of forces and moments. This shift in focus introduces several key challenges that require novel methodologies to address:

- *Control Solutions for Variable Cable Configurations*: In Cable-Driven Wrench Applicators (CDWAs), the primary objective is to exert a desired wrench (a combination of forces and moments) at the end-effector (EE). To achieve this, the system must determine the appropriate set of cable tensions that, when applied, result in the desired wrench. This process is known as *tension distribution selection* or *tension planning*. Robots with different number of cables presents unique challenges for tension distribution [15]. For example, a system with fewer cables may struggle to achieve full controllability, while a system with more cables may face redundancy issues. Developing adaptable control solutions that can handle these variations is critical for ensuring robust performance across different setups.

- *Minimizing Undesired Wrench Components*: When controlling a subset of wrench components (e.g., applying a specific force while ignoring moments), undesired wrench components often emerge as a byproduct [16]. These unintended forces or moments can compromise the system's effectiveness and safety. Addressing this issue requires control strategies that can selectively suppress unwanted wrench components while maintaining the desired output.

- *Ensuring Positive and Bounded Cable Tensions*: Cables can only transmit tensile forces [17], meaning that their tensions must always remain positive. Additionally, these tensions must stay within predefined bounds to avoid cable damage or failure. At the same time, the system must meet pose-dependent force requirements, which can vary significantly across the workspace [18]. Balancing these constraints results in a optimization problem that remains a challenge in the field.

- *Developing Meaningful Performance Metrics*: Traditional performance metrics for position-controlled robots [14] are not sufficient for evaluating wrench application performance. New metrics are needed to capture the system's ability to deliver controlled forces and moments effectively [19]. These metrics should account for factors such as wrench accuracy, cable tensions (and thus energy efficiency), providing a comprehensive assessment of system performance. Beyond evaluating the absolute performance of a robot, these metrics should also allow one to compare the performance of different designs. For example, they should highlight the trade-offs between systems with varying numbers of cables or different cable arrangements, to support the design of such systems.

In summary, the key challenges in cable-driven wrench applicators include: (i) developing adaptable control solutions for varying cable configurations, (ii) minimizing undesired wrench components during force application, (iii) ensuring positive and bounded cable tensions while meeting pose-dependent force requirements, and (iv) establishing meaningful performance metrics for both absolute evaluation and comparative design analysis. Addressing these challenges is essential to advancing the capabilities of CDPRs in force-focused applications.

1.3 Research Objectives and Contributions

This thesis begins to address the challenges outlined in the previous section by introducing a novel analytical framework specifically designed to evaluate and compare the performance of cable-driven wrench applicators. The framework is versatile and can be applied to systems with any number of cables and for any task, with the only condition being the number of cables must exceed the cardinality of the wrench components to be controlled, ensuring cable redundancy. Beyond performance evaluation, the framework enables meaningful comparisons between different robot architectures, offering valuable insights for design optimization. To demonstrate its practical utility, the framework is applied to a real-world scenario, highlighting its strengths and limitations. Additionally, experimental validation is conducted to confirm the consistency and reliability of the proposed approach.

The primary contributions of this work are organized into three key components:

- *Tension Computation Method*: We analyze a method for calculating cable tensions in systems where the number of cables is greater than the wrench components to be controlled. This scenario is common in many practical applications, as it allows for redundancy and greater flexibility in force application. With a geometric approach, we highlight how cable redundancy can be exploited to optimize the performance of the robot.

- *Performance Metrics for Evaluation*: To enable meaningful comparisons between different cable-driven wrench applicators, we introduce three performance metrics:

  – *Overall Performance Index* (OPI), which can be used to guide the selection of the tension planning strategy by evaluating the overall effectiveness of the system in delivering the desired wrench.

  – *Maximum Tension Index (MTI)*, which captures the maximum tension required in the cables, providing insights into the system's energy efficiency and mechanical limits.

  – *Maximum Parasitic-Wrench Index (MPI)*, which quantifies the undesired forces or moments that can arise when controlling only a subset of wrench components. Minimizing these parasitic effects is critical for ensuring precise and safe operation.

- *Practical Application and Validation*: To demonstrate the utility of the framework, we apply it to a real-world rehabilitation robotics scenario. Specifically, we use it to evaluate the feasibility of replacing an 8-cable robot with a simpler 4-cable device, for improved accessibility and mechanical simplicity. This use-case highlights how our framework can be used to evaluate and optimize the design of cable-driven systems for specific applications.

The remainder of this document is structured as follows: Chapter 2 introduces the mathematical foundation for the analysis of cable-driven wrench applicators. Chapter 3 describes the proposed tension computation model for redundant cable-driven wrench applicators and presents its geometric interpretation. Chapter 4 introduces the three performance metrics (OPI, MTI, and MPI) and explains how they are used to evaluate and compare different robot architectures. Chapter 5 presents a practical application of the framework, comparing a 4-cable and an 8-cable robot in a rehabilitation training task. This case study illustrates the framework's ability to provide actionable insights for system design and optimization. Chapter 6 concludes the thesis with a discussion of the findings, limitations, and potential directions for future research.

Chapter 2

Fundamentals of Cable-Driven Wrench Applicators

Cable-Driven Wrench Applicators (CDWAs) apply a specific wrench to the end-effector (EE) by tensioning a set of n cables attached to it. This chapter introduces the geometric and wrench-exertion modeling of a generic CDWA, providing the mathematical framework to compute cable tensions when only a subset of the wrench components requires precise control, while the remaining components, particularly those that could interfere with the task, must be minimized or regulated.

The *geometric model* defines the spatial configuration of the CDWA, including the positions of cable attachment points on the EE and the fixed pulley positions on the frame. This model is crucial for understanding how cable routing influences the EE wrench generation capabilities. Additionally, it provides the foundation for mapping cable tensions to the resultant wrench at the EE, a key step in achieving the desired control objectives.

The *wrench exertion model* focuses on the relationship between cable tensions and forces and moments generated at the EE. To determine the required cable tensions for a given wrench, the *inverse wrench-exertion problem* is solved. In redundant systems, where the number of cables (n) exceeds the number of wrench components to be controlled, the inverse wrench-exertion problem yields an infinite set of feasible tension solutions. In such cases, optimization techniques can be employed to select an optimal tension distribution that enhances system performance while minimizing undesirable wrench components.

2.1 Geometric Model

We consider an inertial reference frame $O(x, y, z)$ and a moving frame $O'(x', y', z')$ attached to the end-effector (EE), as shown in Fig. 2.1. The pose of the EE is defined by its position vector $\mathbf{p}$ in the inertial frame and its orientation, represented by the rotation matrix $\mathbf{R}$. In this work, $\mathbf{R}$ is parameterized using a minimal set of orientation parameters, specifically the tilt and torsion angles $\boldsymbol{\epsilon} = [\phi, \theta, \psi]^\top$ [20].

Each cable is modeled as a massless straight segment guided through an eyelet at point B_i, whose position in the inertial frame is given by the vector $\mathbf{b}_i$. The cable is attached to the EE at point A_i, whose position is expressed in the moving frame as the constant vector $\mathbf{r}'_i$, and the inertial frame as:

$$\mathbf{a}_i = \mathbf{R}\mathbf{r}_i' + \mathbf{p}. \tag{2.1}$$

The closure equation for the i-th cable, describing the relationship between the attachment and routing points, is given by:

$$\mathbf{l}_i = \mathbf{b}_i - \mathbf{a}_i. \tag{2.2}$$

The unit vector defining the cable direction is:

$$\mathbf{t}_i = \frac{\mathbf{l}_i}{\|\mathbf{l}_i\|}. \tag{2.3}$$

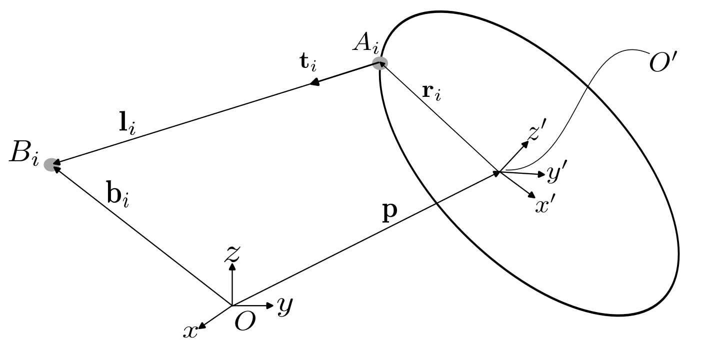

Figure 2.1: Geometric model of the CDWA.

2.1.1 Geometric Problem Formulation

The geometric equations play a crucial role in the analysis and control of CDWAs:

- *Inverse Geometric Problem*: If the EE pose $(\mathbf{p}, \mathbf{R})$ is known, the cable vectors $\mathbf{l}_i$ can be directly computed using Eq. (2.2) for each $i = 1, \ldots, n$.

- *Forward Geometric Problem*: If the cable vectors $\mathbf{l}_i$ are given for all $i = 1, \ldots, n$, solving Eq. (2.2) allows for the determination of the EE position and orientation $(\mathbf{p}, \mathbf{R})$. However, this is only feasible if the number of cables n exceeds the number of degrees of freedom of the EE (tipically 6), ensuring that the system is fully constrained.

In underconstrained systems ($n \leq 6$), the forward geometric problem must be solved in conjunction with static equilibrium equations [21]. However, parallel robot forward kinematics often yield multiple solutions, and numerical methods do not always guarantee convergence [22].

To address these challenges, recent research has investigated the integration of external sensors into the control loop to directly measure the EE pose [23]. Despite this, many robotic systems still rely on camera-based motion capture systems [24] to bypass solving the forward geometric problem. While effective, this remains an expensive solution (see Chapter 5).

2.2 Wrench-Exertion Model

In a Cable-Driven Wrench Applicator (CDWA) with n cables, the applied cable tensions produce a resultant wrench at the end-effector (EE), governed by the following equations:

$$\sum_{i=1}^{n} \mathbf{f}_i = \mathbf{f}_{\text{gen}}, \tag{2.4}$$

$$\sum_{i=1}^{n} \mathbf{r}_i \times \mathbf{f}_i = \mathbf{m}_{\text{gen}}, \tag{2.5}$$

where:

- $\mathbf{f}_i \in \mathbb{R}^3$ is the force exerted by the i-th cable on the EE,
- $\mathbf{f}_{\text{gen}} \in \mathbb{R}^3$ is the force generated on the EE center of mass,
- $\mathbf{m}_{\text{gen}} \in \mathbb{R}^3$ is the moment generated on the EE.

Depending on the application, either all components of $\mathbf{f}_{\text{gen}}$ and $\mathbf{m}_{\text{gen}}$ need to be controlled, or only a subset of them (see Section 2.3).

Since the direction of each cable force $\mathbf{f}_i$ is determined by Eq. (2.3), the equilibrium equations can be rewritten in terms of cable tensions:

$$\sum_{i=1}^{n} \mathbf{t}_i \tau_i = \mathbf{f}_{\text{gen}}, \tag{2.6}$$

$$\sum_{i=1}^{n} (\mathbf{r}_i \times \mathbf{t}_i)\tau_i = \mathbf{m}_{\text{gen}}, \tag{2.7}$$

where τ_i represents the tension magnitude in the i-th cable.

Since Eqs. (2.6) and (2.7) are linear with respect to τ_i, they can be rewritten in matrix form as:

$$\begin{bmatrix} \mathbf{t}_1 & \cdots & \mathbf{t}_n \\ \mathbf{r}_1 \times \mathbf{t}_1 & \cdots & \mathbf{r}_n \times \mathbf{t}_n \end{bmatrix} \begin{bmatrix} \tau_1 \\ \vdots \\ \tau_n \end{bmatrix} = \begin{bmatrix} \mathbf{f}_{\text{gen}} \\ \mathbf{m}_{\text{gen}} \end{bmatrix}. \tag{2.8}$$

Defining:

$$\mathbf{A} = \begin{bmatrix} \mathbf{t}_1 & \cdots & \mathbf{t}_n \\ \mathbf{r}_1 \times \mathbf{t}_1 & \cdots & \mathbf{r}_n \times \mathbf{t}_n \end{bmatrix}, \qquad \mathbf{w} = \begin{bmatrix} \mathbf{f}_{\text{gen}} \\ \mathbf{m}_{\text{gen}} \end{bmatrix}, \tag{2.9}$$

Eq. (2.8) simplifies to:

$$\mathbf{A}\boldsymbol{\tau} = \mathbf{w}, \tag{2.10}$$

which represents the final formulation of the wrench-exertion model for a generic CDWA, capturing the relationship between the tension array $\boldsymbol{\tau} \in \mathbb{R}^n$ and the wrench $\mathbf{w} \in \mathbb{R}^6$ applied to the EE, through the structure matrix $\boldsymbol{A} \in \mathbb{R}^{6\times n}$.

2.3 Solution to the Inverse Wrench-Exertion Problem

To control a Cable-Driven Wrench Applicator (CDWA), the desired wrench at the end-effector (EE) must be converted into cable tensions that the motors will generate. This requires solving the *inverse wrench-exertion problem*, where Eq. (2.10) is solved for the cable tensions.

In wrench-application tasks, the desired wrench $\mathbf{w}$ may be either fully or partially controlled, depending on the number of components that must be regulated. Let m denote the number of *controlled components*. The remaining $s = 6 - m$ components are uncontrolled and can be further categorized based on their impact on the task:

- *Parasitic components* $\mathbf{w}_p \in \mathbb{R}^k$: These hinder the task and negatively affect performance.
- *Residual components* $\mathbf{w}_r \in \mathbb{R}^h$: These are neutral or inconsequential to the task and do not affect performance evaluation.

By definition, the sum of the parasitic and residual components must satisfy:

$$h + k = s. \tag{2.11}$$

For example, if the task requires the control of forces F_x and F_y, then $m = 2$, meaning that $s = 6 - 2 = 4$ components remain uncontrolled.

Moreover, for practical application and physical consistency, the classification of controlled ($\mathbf{w}_c$), residual ($\mathbf{w}_r$), and parasitic ($\mathbf{w}_p$) components of the wrench should be designed so that $\mathbf{w}_c$, $\mathbf{w}_r$ and $\mathbf{w}_p$ consist of either only forces or only moments. This ensures the three wrenches to be homogeneus in terms of units.

To facilitate analysis, we assume that the controlled coordinates appear first in the wrench vector, followed by residual and parasitic components:

$$\mathbf{w} = \left[\mathbf{w}_c^\top\, \mathbf{w}_r^\top\, \mathbf{w}_p^\top\right]^\top. \tag{2.12}$$

Using this partition, Eq. (2.10) can be rewritten as a set of three equations:

$$\mathbf{A}_c \boldsymbol{\tau} = \mathbf{w}_c, \tag{2.13}$$
$$\mathbf{A}_r \boldsymbol{\tau} = \mathbf{w}_r, \tag{2.14}$$
$$\mathbf{A}_p \boldsymbol{\tau} = \mathbf{w}_p, \tag{2.15}$$

where $\mathbf{A}_c \in \mathbb{R}^{m\times n}$, $\mathbf{A}_r \in \mathbb{R}^{h\times n}$, $\mathbf{A}_p \in \mathbb{R}^{k\times n}$. Eqs. (2.13), (2.14) and (2.15) are referred to as *controlled*, *residual*, and *parasitic equilibrium equations*, as they account for controlled, residual and parasitic components of the wrench, respectively. The full structure matrix is given by:

$$\mathbf{A} = \left[\mathbf{A}_c^\top\, \mathbf{A}_r^\top\, \mathbf{A}_p^\top\right]^\top. \tag{2.16}$$

The objective of the *inverse wrench-exertion problem* is to compute the tension array $\boldsymbol{\tau}$ that achieves the desired forces $\mathbf{w}_c$ while keeping $\mathbf{w}_r$ and $\mathbf{w}_p$ within acceptable limits. Additionally, a positivity constraint on cable tensions is required to prevent slack cables. The presence of these bounds makes the inverse wrench-exertion problem a *constrained* problem, whose solution is presented in [25] and is briefly recalled here.

To develop a structured solution, we first consider the unconstrained case, where we temporarily ignore the presence of physical and task-specific bounds. The existence of a solution to the unconstrained inverse wrench-exertion problem depends primarily on the number of cables and the properties of the structure matrix. Since cables can only exert tensile forces, a minimum of $m+1$ cables is required to control m components of the wrench [26]. This establishes a fundamental physical constraint on the number of controllable wrench components:

$$m \leq n-1. \tag{2.17}$$

Additionally, the desired wrench vector $\mathbf{w}_c$ must lie within the subspace spanned by the structure matrix $\mathbf{A}_c$, leading to the condition:

$$\operatorname{rank}(\mathbf{A}_c) = m. \tag{2.18}$$

If both conditions (2.17) and (2.18) are satisfied, the equation

$$\mathbf{A}_c \boldsymbol{\tau} = \mathbf{w}_c \tag{2.19}$$

admits infinitely many solutions for $\boldsymbol{\tau} \in \mathbb{R}^n$, which can be expressed as in [27]:

$$\boldsymbol{\tau} = \boldsymbol{\tau}_p + \mathbf{N}\boldsymbol{\lambda}, \tag{2.20}$$

where:

- $\boldsymbol{\tau}_p = \mathbf{A}_c^{+}\mathbf{w}_c$ is a particular solution,
- $\mathbf{A}_c^{+} \in \mathbb{R}^{n\times m}$ is a right-inverse of $\mathbf{A}_c$,
- $\mathbf{N}$ is a basis for the right null-space (kernel) of $\mathbf{A_c}$,
- $\boldsymbol{\lambda} \in \mathbb{R}^{n-m}$ is a free parameter vector determining a specific element in the null-space.

Matrix $\mathbf{N}$ can be chosen to form an orthonormal basis of the $(n-m)$-dimensional null-space of $\mathbf{A}_c$, such that $\mathbf{N}^\top\mathbf{N} = \mathbb{I}_{n-m}$. Moreover, the particular solution $\boldsymbol{\tau}_p$ satisfies $\mathbf{N}^\top\boldsymbol{\tau}_p = \mathbf{0}_{n-m}$, while the homogeneous solution $\mathbf{N}\boldsymbol{\lambda}$ satisfies $\mathbf{A}_c\mathbf{N}\boldsymbol{\lambda} = \mathbf{0}_{6\times 1}$.

We can now substitute Eq. (2.20) into Eqs. (2.14) and (2.15), obtaining the analytical expression of residual and parasitic components:

$$\mathbf{w}_r = \mathbf{A}_r\left(\boldsymbol{\tau}_p + \mathbf{N}\boldsymbol{\lambda}\right). \tag{2.21}$$

$$\mathbf{w}_p = \mathbf{A}_p\left(\boldsymbol{\tau}_p + \mathbf{N}\boldsymbol{\lambda}\right). \tag{2.22}$$

In the unconstrained case, $\boldsymbol{\lambda}$ is free to take any real value, leading to an *optimization problem*, where the goal is to select an optimal $\boldsymbol{\lambda}$ to achieve desired performance criteria. However, in real applications, due to the presence of task-specific bounds (see Section 3.1), solving for $\boldsymbol{\lambda}$ requires a constrained optimization approach rather than simply selecting an arbitrary null-space solution. Chapter 3 presents a Quadratic Programming (QP) formulation, a well-established technique for solving constrained quadratic optimization problems.

Chapter 3

Tension Distribution Optimization via Quadratic Programming

As introduced in Section 2.3, the inverse wrench-exertion problem of redundant CDWAs requires a constrained optimization method, since it may allow infinite solutions, subjected to some constraints on cable tensions, parasitic and residual effects.

While many options have been explored in the literature [1, 5], this thesis focuses solely on quadratic programming (QP) due to its computational efficiency, ability to prevent discontinuities, and widespread practical use [28]. In this section, we first introduce the typical constraints which bound the solution of the inverse wrench-exertion problem in CDWAs, then we present two quadratic cost functions for computing $\boldsymbol{\lambda}$, each emphasizing key differences between CDWAs performing the same task, as further discussed in Chapter 5:

- *Minimizing the 2-norm of Cable Tensions* (QPT), which prioritizes energy efficiency and safety by reducing overall cable tensions. Lower tensions result in reduced actuator effort, directly decreasing electrical power consumption [29]. From a safety perspective, cable tension is directly related to the system's stiffness. Higher tensions create a stiffer system, which can enhance control precision but may also lead to excessive rigidity, increasing the risk of discomfort or unintended force transmission to the patient [30]. By reducing cable tensions, the system becomes more compliant, allowing for safer and more adaptive interactions between the robot and the user. This reduces the risk of excessive force application while improving the overall comfort and safety of the rehabilitation process.
- *Minimizing the 2-norm of Parasitic Components* (QPP), which aims to minimize undesired wrench components.

Subsequently, we introduce a graphical tool for geometrically analyzing the solution space of CDWAs with n=m+2 cables. This tool provides an alternative representation of the constrained optimization problem and visualizes the two distinct solutions obtained from QPT and QPP.

3.1 Optimization constraints

Cable-Driven Wrench-Applicators rely on cables to apply wrench to a platform or end-effector. Enforcing constraints on cable tensions and parasitic wrench is essential for ensuring feasibility, safety, and performance. These constraints prevent cables from going slack or exceeding their strength limits and help maintain stable and precise operation [31]. By bounding tensions and parasitic wrenches, the system remains within a safe and controllable regime [31].

A key requirement in CDWAs is that cables can only exert tensile forces [17]. If a cable's tension drops to zero or below (non physical), it slackens, leading to loss of actuation, reduced control accuracy, and potential mechanical failure due improper spooling. To prevent these issues, a lower bound on tension is imposed:

$$\tau_i \geq \tau_{\min}, \quad \forall i. \tag{3.1}$$

The value of $\tau_{\min}$ is chosen to account for cable weight, elasticity, and expected disturbances, ensuring a baseline level of stiffness and control.

At the same time, an upper bound on tension prevents excessive forces that could damage the system [32]:

$$\tau_i \leq \tau_{\max}, \quad \forall i. \tag{3.2}$$

Exceeding $\tau_{\max}$ risks cable failure, actuator overload, or excessive power consumption. The value of $\tau_{\max}$ can be set based on the weakest component in the system, whether it is the cable, actuator, or supporting structure, or based on energetic considerations.

Beyond tension constraints, the parasitic wrench must also be limited. Unintended forces or moments can introduce instability, compromise precision, and reduce performance in applications such as rehabilitation robotics and precision manipulation [16]. A bound is imposed to keep these disturbances within an acceptable range:

$$\mathbf{w}_p \leq \mathbf{w}_{p,\max}. \tag{3.3}$$

The threshold $\mathbf{w}_{p,\max}$ is determined based on the application's sensitivity to external disturbances, ensuring reliable operation.

Finally, for some applications, a constraint on the residual wrench might also be required, although, by definition, $\mathbf{w}_r$ does not hinder the task at hand. Typically, the residual wrench is constrained for safety reasons with relatively larger bounds than $\mathbf{w}_p$, as Chapter 5 will show. Similarly to $\mathbf{w}_p$, the constrain on the residual wrench can be expressed as:

$$\mathbf{w}_r \leq \mathbf{w}_{r,\max}. \tag{3.4}$$

These constraints significantly impact the solution space of the inverse wrench-exertion problem. As highlighted in Section 2.3, multiple feasible tension distributions exist for a given desired wrench. However, enforcing constraints such as $\tau_{\min} \leq \tau_i \leq \tau_{\max}$ and $\mathbf{w}_p \leq \mathbf{w}_{p,\max}$ reduces the solution set to only physically achievable and safe configurations.

3.2 Optimization cost functions: QPT and QPP

The *quadratic programming tension* (QPT) cost function aims at minimizing the 2-norm of cable tensions and is derived from Eq. (2.20) as:

$$\|\boldsymbol{\tau}(\boldsymbol{\lambda})\|_2 = \boldsymbol{\lambda}^\top \mathbf{H} \boldsymbol{\lambda} + 2\mathbf{f}^\top \boldsymbol{\lambda} + g, \tag{3.5}$$

with:

$$\mathbf{H} = \mathbf{N}^\top \mathbf{N}, \quad \mathbf{f} = \mathbf{N}^\top \boldsymbol{\tau}_p \quad g = \boldsymbol{\tau}_p^\top \boldsymbol{\tau}_p.$$

As highlighted in Section 2.3, $\mathbf{N}^\top\mathbf{N} = \mathbb{I}_m$ and $\mathbf{N}^\top\boldsymbol{\tau}_p = \mathbf{0}_{n-m}$, and (3.5) can be rewritten as:

$$\|\boldsymbol{\tau}(\boldsymbol{\lambda})\|_2 = \boldsymbol{\lambda}^\top\boldsymbol{\lambda} + g. \tag{3.6}$$

where g is a constant for a given pose of the EE. While g remains part of the cost function, it does not affect the optimization process since its gradient is zero. Thus, minimizing $\|\boldsymbol{\tau}(\boldsymbol{\lambda})\|_2$ is equivalent to minimizing:

$$\|\boldsymbol{\tau}(\boldsymbol{\lambda})\|_2 = \boldsymbol{\lambda}^\top\boldsymbol{\lambda} \tag{3.7}$$

which represents the final formulation of the quadratic cost function associated to the 2-$norm$ of cable tensions. Although g is not explicitly included in the optimization, it is still part of the full cost function definition.

The QPT optimization problem can be formulated as:

$$\begin{aligned} \min_{\boldsymbol{\lambda}} \quad & \|\boldsymbol{\tau}(\boldsymbol{\lambda})\|_2 \\ \text{s.t.} \quad & \begin{bmatrix}\mathbf{A}_p \\ \mathbf{A}_r\end{bmatrix}\boldsymbol{\tau}(\boldsymbol{\lambda}) \leq \begin{bmatrix}\mathbf{w}_{p,\max} \\ \mathbf{w}_{r,\max}\end{bmatrix}, \\ & \boldsymbol{\tau}_{\min} \preceq \boldsymbol{\tau}(\boldsymbol{\lambda}) \preceq \boldsymbol{\tau}_{\max}. \end{aligned} \tag{3.8}$$

where $\preceq$ refers to element-wise inequalities, $\mathbf{w}_{p,\max}$ and $\mathbf{w}_{r,\max}$ are the vectors holding maximum values of parasitic and residual wrench components, respectively, and $\tau_{\min}$ and $\tau_{\max}$ are lower and upper cable tension limits, respectively.

Alternatively to QPT, we can compute $\boldsymbol{\lambda}$ with *quadratic programming parasitic components* (QPP). The corresponding cost function can be found from Eq. (2.22) as:

$$\|\mathbf{w}_p(\boldsymbol{\lambda})\|_2 = \boldsymbol{\lambda}^\top\mathbf{L}\boldsymbol{\lambda} + 2\mathbf{p}^\top\boldsymbol{\lambda} + c, \tag{3.9}$$

with:

$$\mathbf{L} = \mathbf{N}^\top\mathbf{A}_p^\top\mathbf{A}_p\mathbf{N}, \quad \mathbf{p} = \mathbf{N}^\top\mathbf{A}_p^\top\mathbf{A}_p\boldsymbol{\tau}_p, \quad c = \boldsymbol{\tau}_p^\top\mathbf{A}_p^\top\mathbf{A}_p\boldsymbol{\tau}_p.$$

Similarly to QPT, c is a constant for a given EE pose and its gradient is zero, thus can be eliminated for simplicity from the optimization, yielding to:

$$\|\mathbf{w}_p(\boldsymbol{\lambda})\|_2 = \boldsymbol{\lambda}^\top\mathbf{L}\boldsymbol{\lambda} + 2\mathbf{p}^\top\boldsymbol{\lambda}, \tag{3.10}$$

and the QPP optimization problem can be formulated as:

$$\begin{aligned} \min_{\boldsymbol{\lambda}} \quad & \|\mathbf{w}_p(\boldsymbol{\lambda})\|_2 \\ \text{s.t.} \quad & \mathbf{A}_r\boldsymbol{\tau}(\boldsymbol{\lambda}) \leq \mathbf{w}_{r,\max}, \\ & \boldsymbol{\tau}_{\min} \preceq \boldsymbol{\tau}(\boldsymbol{\lambda}) \preceq \boldsymbol{\tau}_{\max}. \end{aligned} \tag{3.11}$$

The presented QPT and QPP optimization problems can be solved numerically in MATLAB, for instance, using the `quadprog` function. Once $\boldsymbol{\lambda}$ is obtained from either QPT or QPP, the tension distribution $\boldsymbol{\tau}$ can be computed using Eq. (2.20), the residual wrench $\mathbf{w}_r$ from Eq. (2.21), and the parasitic wrench $\mathbf{w}_p$ via Eq. (2.22).

However, an analytical solution to the constrained optimization problem also exists, based on the Karush-Kuhn-Tucker (KKT) conditions. This formulation can be leveraged to develop efficient algorithms that determine a closed-form solution with minimal numerical iterations, provided that the dimension of $\boldsymbol{\lambda}$ remains small, typically 1 or 2. The next subsection reviews a well-known algorithm originally designed for CDWAs with $n = m + 2$ cables to solve the QPT optimization problem. We then demonstrate how this algorithm can be extended to derive the closed-form solution for QPP as well.

3.3 Geometric approach for robots with m+2 cables

The analytical solution of constrained optimization problems using the Karush-Kuhn-Tucker (KKT) conditions is well established in the literature [33] and can be employed to solve such problems efficiently. However, deriving an analytical solution can be challenging, particularly when the constraints are non linear or the problem is high-dimensional.

In this section, we review [27], a versatile algorithm developed for CDWAs with $n = m+2$ cables, where m denotes the number of components of the controlled wrench vector $\mathbf{w}_c$. This algorithm (i) finds the feasible polygon, namely the set of feasible values of $\boldsymbol{\lambda}$ which satisfy the problem's constraints, and (ii) leverages KKT conditions to derive a closed-form solution of the QPT optimization problem, while requiring minimal numerical iterations, making it a fast hybrid numerical-analytical approach feasible for real-time implementation. We will demonstrate how this algorithm can be extended to address QPP as well. Finally, we will interpret the QPT and QPP solutions geometrically, to highlight relevant properties of both options.

For the sake of simplicity, in this section we will consider the constraints on cable tensions only (3.1)-(3.2), while neglecting those regarding parasitic and residual wrench (3.3)-(3.4).

3.3.1 Feasible tension polygon

For CDWAs with $n = m+2$ cables, with m being the cardinality of the controlled wrench $\mathbf{w}_c$, the solution space of Eq.(2.20) is the vector subspace $\mathbf{P} \subset \mathbb{R}^2$, defined as in [27]:

$$\mathbf{P} = \{\boldsymbol{\lambda} \in \mathbb{R}^2 \mid \tau_{\min} \leq \tau_p + \mathbf{N}\boldsymbol{\lambda} \leq \tau_{\max}\}. \tag{3.12}$$

$\mathbf{P}$ is referred to as *feasible tension polygon*, as it contains all the possible sets $\boldsymbol{\lambda} = [\lambda_1, \lambda_2]^\top$ that, through Eq. (2.20), generate a tension distribution $\boldsymbol{\tau}$ which satisfies the tension constraints. In fact, substituting Eq.(2.20) into the constrain equations (3.1) and (3.2), one obtaines a system of $2n$ linear inequalities:

$$\boldsymbol{\tau}_{min} - \boldsymbol{\tau}_p \leq \mathbf{N}\boldsymbol{\lambda} \leq \boldsymbol{\tau}_{max} - \boldsymbol{\tau}_p \tag{3.13}$$

which can be explicitly written as:

$$\begin{aligned}
\mathbf{n}_1\boldsymbol{\lambda} &\geq \tau_{min} - \tau_{p,1},\\
\mathbf{n}_1\boldsymbol{\lambda} &\leq \tau_{max} - \tau_{p,1},\\
\mathbf{n}_2\boldsymbol{\lambda} &\geq \tau_{min} - \tau_{p,2},\\
&\vdots\\
\mathbf{n}_n\boldsymbol{\lambda} &\leq \tau_{max} - \tau_{p,n},
\end{aligned} \tag{3.14}$$

where $\mathbf{n}_i$ $(1x2)$ is the i-th row of matrix $\mathbf{N}$, τ_{min} and τ_{max} are the lower and upper tension bounds, respectively, and $\tau_{p,i}$ is the i-th element of $\boldsymbol{\tau}_p$, with $i = 1,..,n$. Each

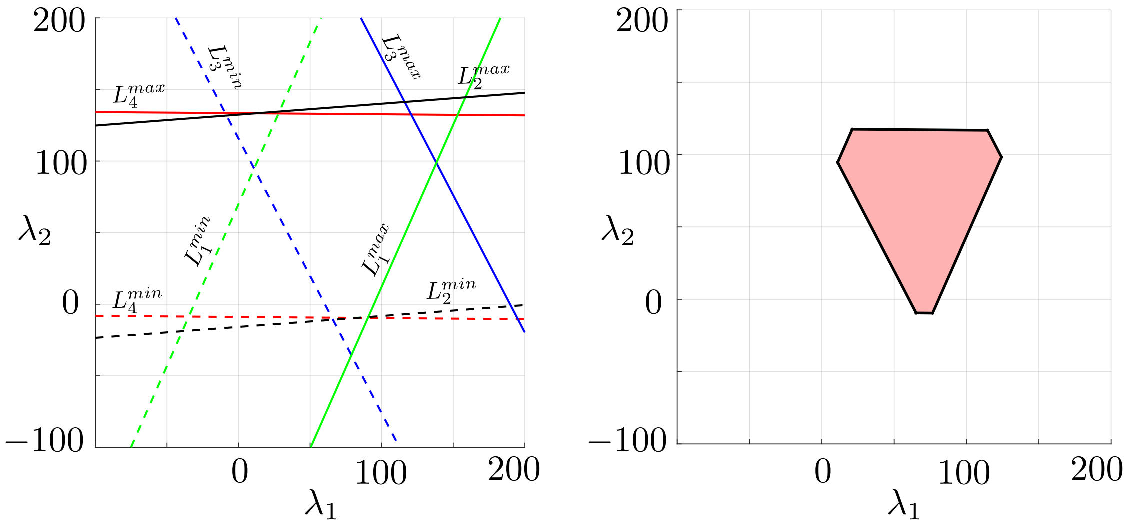

(a) Inequality lines

(b) Feasible tension polygon

Figure 3.1: Example of feasible tension polygon of a 4-cable wrench applicator with the EE in a certain pose.

inequality defines a half-plane bounded by a line corresponding to values of $\boldsymbol{\lambda}$ for which one cable tension is equal to τ_{min} or τ_{max}. Such lines can be identified simply by turning the inequalities into equalities, and will be referred to as *inequality lines* $L_1^{min}, L_1^{max}, L_2^{min}, ..., L_n^{max}$ (See Fig. 3.1a). The intersection of the $2n$ half-planes in (3.14) forms the feasible tension polygon $\mathbf{P}$ (Fig. 3.1b). In [27], a versatile algorithm is presented to determine the edges of the feasible polygon $\mathbf{P}$ for CDWAs with n=m+2 cables. It is shown that, after a finite number of iterations, the algorithm will complete the identification of $\mathbf{P}$ with two possible outcomes: if a convex feasible polygon is found, its vertices will be returned, otherwise $\mathbf{P} = \emptyset$, namely $\nexists\, \boldsymbol{\lambda} \in \mathbb{R}^2 \mid \{\tau_{\min} \leq \tau_p + \mathbf{N}\boldsymbol{\lambda} \leq \tau_{\max}\}$ and Eq.(2.10) has no solution.

3.3.2 Closed-form QPT Solution

This subsection presents a method to determine the tension distribution given by QPT in closed form with a few and finite numerical iterations, assuming that the feasible polygon $\mathbf{P}$ is known. It is further assumed that $\mathbf{P}$ is nonempty, as otherwise, no feasible tension distribution exists.

As highlighted in Eq. (3.8), the QPT problem is formulated as:

$$\begin{aligned} \min_{\boldsymbol{\lambda}} \quad & \boldsymbol{\lambda}^\top \boldsymbol{\lambda} \\ \text{s.t.} \quad & \boldsymbol{\tau}_{\min} - \boldsymbol{\tau}_p \leq \mathbf{N}\boldsymbol{\lambda} \leq \boldsymbol{\tau}_{\max} - \boldsymbol{\tau}_p. \end{aligned} \tag{3.15}$$

This is a strictly convex quadratic optimization problem with a unique global solution [27]. The quadratic form $\boldsymbol{\lambda}^\top \boldsymbol{\lambda}$ is a circle centered at the origin. If the origin $\boldsymbol{\lambda} = \mathbf{0}$ lies within the feasible tension polygon $\mathbf{P}$, it is the optimal solution to Eq. (3.15), with the corresponding tension distribution given by $\boldsymbol{\tau}_p = \mathbf{A}_c^+ \mathbf{w}_c$ (Fig. 3.2). However, if $\mathbf{0} \notin \mathbf{P}$, the optimal solution must lie on the boundary of $\mathbf{P}$ (Fig. 3.3), and can be determined using the Karush-Kuhn-Tucker (KKT) conditions iterating over the polygon's vertices and edges.

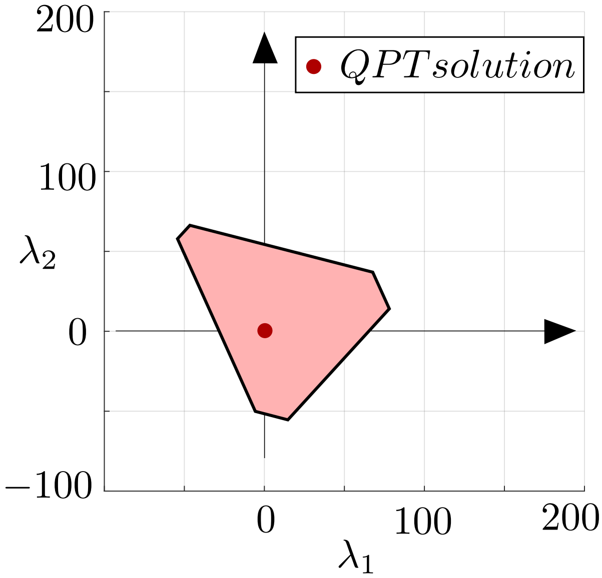

Figure 3.2: Example of a scenario where $\mathbf{0} \in \mathbf{P}$

3.3.2.1 Vertex Optimality Condition

The vertex optimality check is performed using the Karush-Kuhn-Tucker (KKT) conditions, which provide necessary conditions for a solution to be optimal under constraints (see Appendix A).

A vertex $\mathbf{v}_{ij} \in \mathbf{P}$ is formed at the intersection of two constraint lines, denoted as L_i and L_j, which are derived by turning inequalities into equalities:

$$L_i: \quad \mathbf{n}_i \boldsymbol{\lambda} = b_i - \tau_{p,i}, \tag{3.16}$$
$$L_j: \quad \mathbf{n}_j \boldsymbol{\lambda} = b_j - \tau_{p,j}, \tag{3.17}$$

where $\mathbf{n}_i$ is the i-th row of the matrix $\mathbf{N}$, and b_i corresponds to either $\tau_{\min}$ or $\tau_{\max}$, depending on whether L_i represents a lower or upper bound. The same applies to L_j with index j.

To determine whether a given vertex is optimal, we formulate the Lagrangian of the problem as:

$$\mathscr{L}(\boldsymbol{\lambda}, \mu_i, \mu_j) = \boldsymbol{\lambda}^\top \boldsymbol{\lambda} + \mu_i(\mathbf{n}_i \boldsymbol{\lambda} - (b_i - \tau_{p,i})) + \mu_j(\mathbf{n}_j \boldsymbol{\lambda} - (b_j - \tau_{p,j})), \tag{3.18}$$

where μ_i and μ_j are the Lagrange multipliers associated with the active constraints L_i and L_j, respectively.

Applying the stationarity condition, which ensures that the gradient of the Lagrangian with respect to $\boldsymbol{\lambda}$ is zero, we obtain:

$$\nabla_{\boldsymbol{\lambda}} \mathscr{L}(\boldsymbol{\lambda}, \mu_i, \mu_j) = 2\boldsymbol{\lambda} + \mathbf{n}_i^\top \mu_i + \mathbf{n}_j^\top \mu_j = \mathbf{0}, \tag{3.19}$$

which leads to:

$$\begin{bmatrix} \mathbf{n}_i^\top & \mathbf{n}_j^\top \end{bmatrix} \begin{bmatrix} \mu_i \\ \mu_j \end{bmatrix} = -2\boldsymbol{\lambda}. \tag{3.20}$$

where $[\mathbf{n}_i^\top \quad \mathbf{n}_j^\top]$ is a $(2x2)$ square matrix.

To facilitate a structured approach, we introduce the scaled constraint normals:

$$\boldsymbol{a}_i = s_i \mathbf{n}_i^\top, \quad \boldsymbol{a}_j = s_j \mathbf{n}_j^\top, \tag{3.21}$$

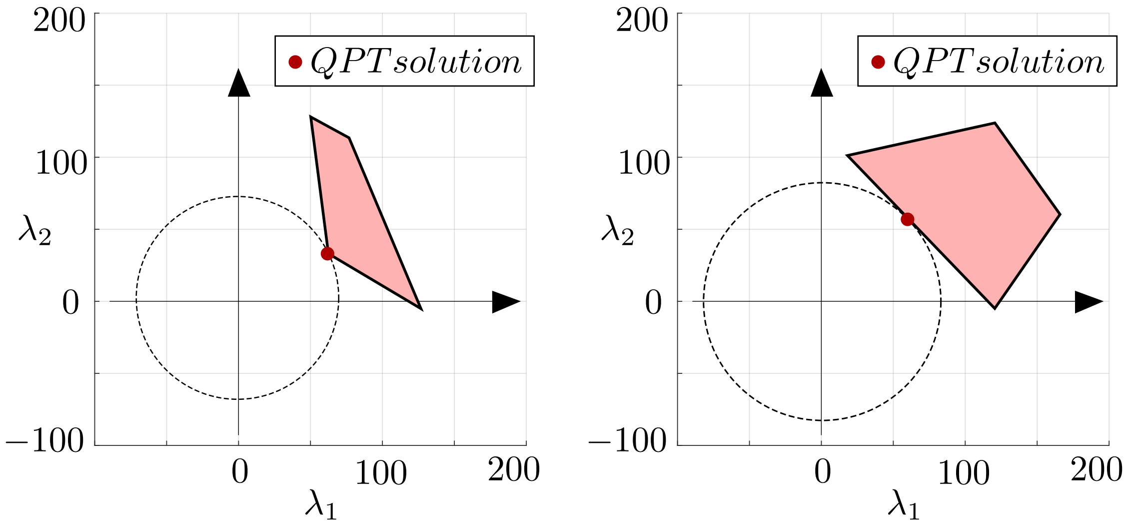

(a) Vertex optimality (b) Edge optimality

Figure 3.3: Example of two scenarios where $\mathbf{0} \notin \mathbf{P}$.

where the scaling factors s_i and s_j are defined as:

$$s_i = \begin{cases} -1, & \text{if} \quad b_i = \tau_{\max}, \\ 1, & \text{if} \quad b_i = \tau_{\min}. \end{cases}$$

and similarly for s_j. The introduction of $\boldsymbol{a}_i$ ensures a consistent sign convention when handling constraints.

Using these definitions, we rewrite Eq. (3.20) in terms of the vertex currently being explored, $\mathbf{v}_{ij}$, as:

$$\begin{bmatrix} \mu_i \\ \mu_j \end{bmatrix} = [\boldsymbol{a}_i \quad \boldsymbol{a}_j]^{-1}\mathbf{v}_{ij}. \tag{3.22}$$

The dual feasibility conditions require that all Lagrange multipliers associated with active constraints are non-negative:

$$\begin{cases} \mu_i \geq 0, \\ \mu_j \geq 0. \end{cases}$$

If both conditions hold, the vertex $\mathbf{v}_{ij} \in \mathbf{P}$ is the optimal solution to Eq. (3.15)[1].

An example of a vertex satisfying optimality conditions is shown in Fig. 3.3a.

3.3.2.2 Edge Optimality Condition

If the vertex $\mathbf{v}_{ij} \in \mathbf{P}$ is not optimal, the search proceeds along the next edge of $\mathbf{P}$, defined as the segment of L_j connecting the vertices $\mathbf{v}_{ij}$ and $\mathbf{v}_{jk} \in \mathbf{P}$.

From Eq. (3.17), the Lagrangian function for this optimization step is:

$$\mathscr{L}(\boldsymbol{\lambda}, \mu_j) = \boldsymbol{\lambda}^\top \boldsymbol{\lambda} + \mu_j(\mathbf{n}_j \boldsymbol{\lambda} - (b_j - \tau_{p,j})), \tag{3.23}$$

[1] In the general formulation presented in Appendix A, the vertex $\mathbf{v}_{ij} \in \mathbf{P}$ inherently satisfies primal feasibility, while the absence of inequality constraints ensures that the complementary slackness condition holds automatically.

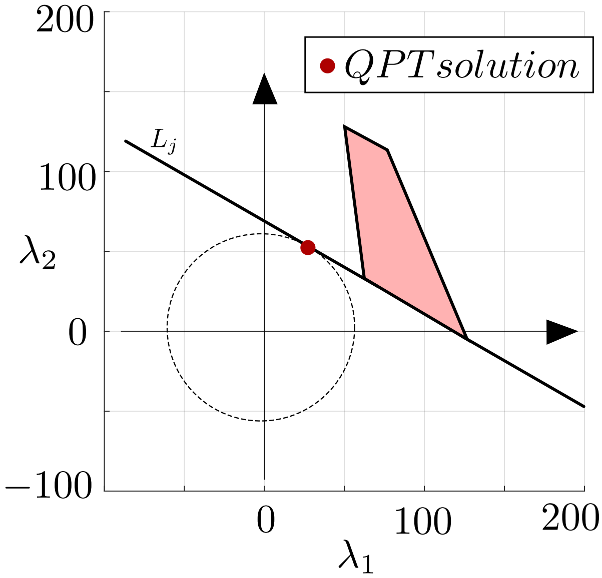

Figure 3.4: Example of QPT unfeasible edge search ($\boldsymbol{\lambda} \notin \mathbf{P}$) along inequality line L_j.

where μ_j is the Lagrange multiplier associated with the active constraint L_j.

Applying the stationarity condition by setting the gradient of the Lagrangian to zero, we obtain:

$$\nabla_{\boldsymbol{\lambda}} \mathscr{L}(\boldsymbol{\lambda}, \mu_j) = 2\boldsymbol{\lambda} + \mathbf{n}_j^\top \mu_j = \mathbf{0}, \tag{3.24}$$

which simplifies to:

$$\boldsymbol{\lambda} = -\frac{\mu_j \mathbf{n}_j^\top}{2}. \tag{3.25}$$

To ensure consistency in handling constraints, we introduce:

$$\boldsymbol{a}_j = s_j \mathbf{n}_j^\top, \tag{3.26}$$

where s_j is defined as:

$$s_j = \begin{cases} -1, & \text{if} \quad b_j = \tau_{\max}, \\ 1, & \text{if} \quad b_j = \tau_{\min}. \end{cases}$$

Substituting $\boldsymbol{\lambda}$ into Eq. (3.17), we solve for μ_j:

$$\mu_j = \frac{2s_j(b_j - \tau_{p,j})}{\boldsymbol{a}_j^\top \boldsymbol{a}_j}. \tag{3.27}$$

The solution satisfies optimality if the dual feasibility condition holds:

$$\mu_j \geq 0. \tag{3.28}$$

If Eq. (3.28) is satisfied, the optimal solution along the edge is:

$$\boldsymbol{\lambda} = \frac{\mu_j \boldsymbol{a}_j}{2}. \tag{3.29}$$

Before confirming that $\boldsymbol{\lambda}$ from Eq. (3.29) is the optimal solution to Eq. (3.15), it is necessary to verify that the primal feasibility condition holds, ensuring that the solution satisfies all constraints of the problem[2]. Specifically, we must check whether $\boldsymbol{\lambda}$ lies within the segment of L_j bounded by $\mathbf{v}_{ij}$ and $\mathbf{v}_{jk}$:

[2] In the general formulation presented in Appendix A, the complementary slackness condition holds automatically due to the absence of inequality constraints.

$$\boldsymbol{\lambda} \in [\mathbf{v}_{ij}, \mathbf{v}_{jk}]. \tag{3.30}$$

This verification can be performed by substituting Eq. (3.29) into Eq. (3.13) and ensuring that all $2n$ inequality constraints are satisfied.

If the solution is found to be infeasible, the point defined by Eq. (3.29) must be discarded, and the search for the optimal solution continues by exploring the next vertices and edges of **P**.

An example of edge optimality is illustrated in Fig. 3.3b, while an instance of infeasibility is shown in Fig. 3.4.

3.3.3 Closed-form QPP Solution

This subsection presents a method to determine the tension distribution given by QPP in closed form with a few numerical iterations, assuming that the feasible polygon **P** is known. It is further assumed that **P** is nonempty, as otherwise, no feasible tension distribution exists.

As highlighted in Eq. (3.11), the QPP problem is formulated as:

$$\begin{aligned} \min_{\boldsymbol{\lambda}} \quad & \boldsymbol{\lambda}^\top \mathbf{L} \boldsymbol{\lambda} + 2\mathbf{p}^\top \boldsymbol{\lambda} \\ \text{s.t.} \quad & \boldsymbol{\tau}_{\min} - \boldsymbol{\tau}_p \le \mathbf{N}\boldsymbol{\lambda} \le \boldsymbol{\tau}_{\max} - \boldsymbol{\tau}_p. \end{aligned} \tag{3.31}$$

This is a strictly convex quadratic optimization problem with a unique global solution [27].

Since matrix **L** is a (2x2) positive definite, the quadratic form $\boldsymbol{\lambda}^\top \mathbf{L} \boldsymbol{\lambda} + 2\mathbf{p}^\top \boldsymbol{\lambda}$ is a 2-D ellipsoid, i.e. an ellipse. The center of this ellipse minimizes the cost function and corresponds to the unconstrained optimal solution. It can be found minimizing Eq. (3.10):

$$\nabla_{\boldsymbol{\lambda}} \|\mathbf{w}_p(\boldsymbol{\lambda})\|_2 = 2\mathbf{L}\boldsymbol{\lambda} + 2\mathbf{p} = \mathbf{0}, \tag{3.32}$$

yielding:

$$\boldsymbol{\lambda}_c = -\mathbf{L}^{-1}\mathbf{p}. \tag{3.33}$$

If $\boldsymbol{\lambda}_c$ lies within **P**, it is a feasible solution and represents the global optimum of Eq. (3.31)(Fig. 3.5). Conversely, if $\boldsymbol{\lambda}_c \notin \mathbf{P}$, the optimal solution must lie on the boundary of **P** (Fig. 3.6), and can be determined using the Karush-Kuhn-Tucker (KKT) conditions iterating over the polygon's vertices and edges.

3.3.3.1 Vertex Optimality Condition

The vertex optimality check is performed using the Karush-Kuhn-Tucker (KKT) conditions, which provide necessary conditions for a solution to be optimal under constraints (see Appendix A).

A vertex $\mathbf{v}_{ij} \in \mathbf{P}$ is formed at the intersection of two constraint lines, denoted as L_i and L_j, which are derived by turning inequalities into equalities:

$$L_i: \quad \mathbf{n}_i \boldsymbol{\lambda} = b_i - \tau_{p,i}, \tag{3.34}$$

$$L_j: \quad \mathbf{n}_j \boldsymbol{\lambda} = b_j - \tau_{p,j}. \tag{3.35}$$

where $\mathbf{n}_i$ is the i-th row of matrix **N**, and b_i corresponds to either $\tau_{\min}$ or $\tau_{\max}$, depending on whether L_i represents a lower or upper bound. The same definitions apply to L_j for index j.

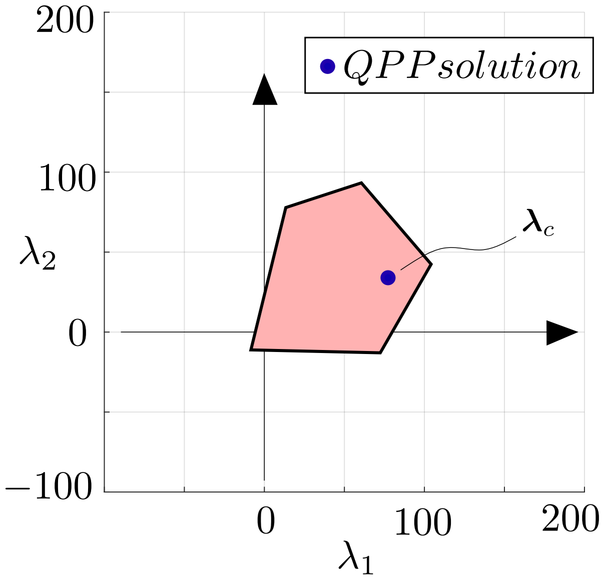

Figure 3.5: Example of a scenario where $\boldsymbol{\lambda}_c \in \mathbf{P}$

To determine whether a given vertex is optimal, we construct the Lagrangian function:

$$\mathscr{L}(\boldsymbol{\lambda}, \mu_i, \mu_j) = \boldsymbol{\lambda}^\top \mathbf{L}\boldsymbol{\lambda} + 2\mathbf{p}^\top \boldsymbol{\lambda} + \mu_i(\mathbf{n}_i \boldsymbol{\lambda} - (b_i - \tau_{p,i})) + \mu_j(\mathbf{n}_j \boldsymbol{\lambda} - (b_j - \tau_{p,j})), \tag{3.36}$$

where μ_i and μ_j are the Lagrange multipliers associated with the active constraints L_i and L_j, respectively.

Applying the stationarity condition by setting the gradient of the Lagrangian with respect to $\boldsymbol{\lambda}$ to zero, we obtain:

$$\nabla_{\boldsymbol{\lambda}} \mathscr{L}(\boldsymbol{\lambda}, \mu_i, \mu_j) = 2\mathbf{L}\boldsymbol{\lambda} + 2\mathbf{p} + \mathbf{n}_i^\top \mu_i + \mathbf{n}_j^\top \mu_j = \mathbf{0}. \tag{3.37}$$

which leads to:

$$\begin{bmatrix} \mathbf{n}_i^\top & \mathbf{n}_j^\top \end{bmatrix} \begin{bmatrix} \mu_i \\ \mu_j \end{bmatrix} = -2(\mathbf{L}\boldsymbol{\lambda} + \mathbf{p}). \tag{3.38}$$

where $[\mathbf{n}_i^\top \quad \mathbf{n}_j^\top]$ is a $(2x2)$ square matrix.

To simplify handling of constraints, we introduce the scaled constraint normals:

$$\boldsymbol{a}_i = s_i \mathbf{n}_i^\top, \quad \boldsymbol{a}_j = s_j \mathbf{n}_j^\top, \tag{3.39}$$

where the scaling factors s_i and s_j are defined as:

$$s_i = \begin{cases} -1, & \text{if} \quad b_i = \tau_{\max}, \\ 1, & \text{if} \quad b_i = \tau_{\min}. \end{cases}$$

and similarly for s_j. The introduction of $\boldsymbol{a}_i$ ensures a consistent sign convention when handling constraints.

Using these definitions, Eq. (3.38) can be solved in closed form for the Lagrange multipliers:

$$\begin{bmatrix} \mu_i \\ \mu_j \end{bmatrix} = [\boldsymbol{a}_i \quad \boldsymbol{a}_j]^{-1}(\mathbf{L}\mathbf{v}_{ij} + \mathbf{p}). \tag{3.40}$$

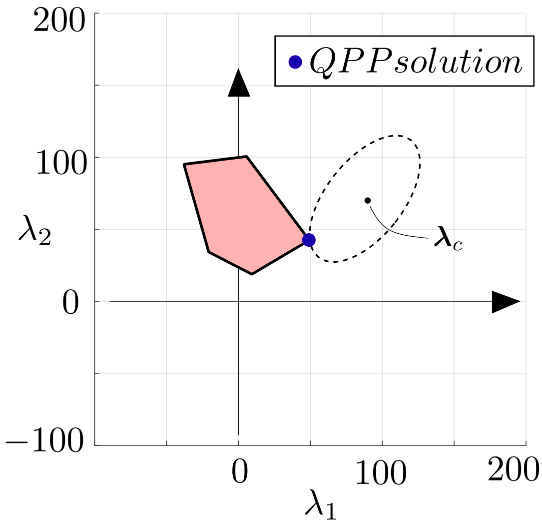

(a) Vertex optimality

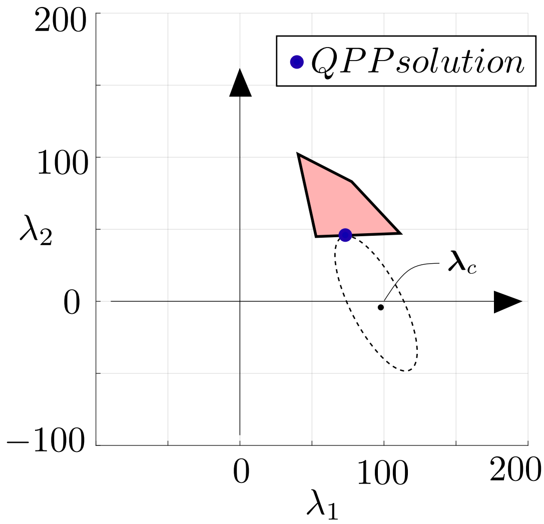

(b) Edge optimality

Figure 3.6: Example of two scenarios where $\boldsymbol{\lambda}_c \notin \mathbf{P}$.

The dual feasibility conditions require that all Lagrange multipliers remain non-negative:

$$\begin{cases} \mu_i \geq 0, \\ \mu_j \geq 0. \end{cases}$$

If both conditions hold, the vertex $\mathbf{v}_{ij} \in \mathbf{P}$ is the optimal solution to Eq. (3.31)[3].

An example of a vertex satisfying optimality conditions is shown in Fig. 3.6a.

3.3.3.2 Edge Optimality Condition

If the vertex $\mathbf{v}_{ij} \in \mathbf{P}$ is not optimal, the search proceeds along the next edge of $\mathbf{P}$, defined as the segment of L_j connecting the vertices $\mathbf{v}_{ij}$ and $\mathbf{v}_{jk} \in \mathbf{P}$.

From Eq. (3.35), the Lagrangian function for this optimization step is:

$$\mathscr{L}(\boldsymbol{\lambda}, \mu_j) = \boldsymbol{\lambda}^\top \mathbf{L}\boldsymbol{\lambda} + 2\mathbf{p}^\top \boldsymbol{\lambda} + \mu_j(\mathbf{n}_j \boldsymbol{\lambda} - (b_j - \tau_{p,j})), \tag{3.41}$$

where μ_j is the Lagrange multiplier associated with the active constraint L_j.

Applying the stationarity condition, we set the gradient of the Lagrangian to zero:

$$\nabla_{\boldsymbol{\lambda}} \mathscr{L}(\boldsymbol{\lambda}, \mu_j) = 2\mathbf{L}\boldsymbol{\lambda} + 2\mathbf{p} + \mathbf{n}_j^\top \mu_j = \mathbf{0}, \tag{3.42}$$

which leads to:

$$\boldsymbol{\lambda} = -\mathbf{L}^{-1}(\mathbf{p} + \frac{\mu_j \mathbf{n}_j^\top}{2}). \tag{3.43}$$

To ensure consistent handling of constraints, we introduce:

$$\boldsymbol{a}_j = s_j \mathbf{n}_j^\top, \tag{3.44}$$

[3] In the general formulation presented in Appendix A, the vertex $\mathbf{v}_{ij} \in \mathbf{P}$ inherently satisfies primal feasibility, while the absence of inequality constraints ensures that the complementary slackness condition holds automatically.

where the scaling factor s_j is defined as:

$$s_j = \begin{cases} -1, & \text{if} \quad b_j = \tau_{\max}, \\ 1, & \text{if} \quad b_j = \tau_{\min}. \end{cases}$$

Substituting Eq. (3.43) into Eq. (3.35), we solve for μ_j:

$$\mu_j = \frac{2s_j(\mathbf{n}_j\mathbf{L}^{-1}\mathbf{p} + b_j - \tau_{p,j})}{\boldsymbol{a}_j^\top \mathbf{L}^{-1}\boldsymbol{a}_j}. \tag{3.45}$$

The solution satisfies optimality if the dual feasibility condition holds:

$$\mu_j \geq 0. \tag{3.46}$$

If Eq. (3.46) is satisfied, the optimal solution along the edge is:

$$\boldsymbol{\lambda} = -\mathbf{L}^{-1}(\mathbf{p} - \frac{\boldsymbol{a}_j\mu_j}{2}). \tag{3.47}$$

Before confirming that $\boldsymbol{\lambda}$ from Eq. (3.47) is the optimal solution to Eq. (3.31), it is necessary to verify that the primal feasibility condition holds, ensuring that the solution satisfies all constraints of the problem[4]. Specifically, we must check whether $\boldsymbol{\lambda}$ lies within the segment of L_j bounded by $\mathbf{v}_{ij}$ and $\mathbf{v}_{jk}$:

$$\boldsymbol{\lambda} \in [\mathbf{v}_{ij}, \mathbf{v}_{jk}]. \tag{3.48}$$

This verification can be performed by substituting Eq. (3.47) into Eq. (3.13) and ensuring that all $2n$ inequality constraints are satisfied.

If the solution is found to be infeasible, the point defined by Eq. (3.47) must be discarded, and the search for the optimal solution continues by exploring the next vertices and edges of $\mathbf{P}$.

An example of edge optimality is illustrated in Fig. 3.6b, while an instance of infeasibility is shown in Fig. 3.7.

3.3.4 Geometric interpretation of QPT and QPP

The Quadratic Programming Tension (QPT) defines a cost function with circular level sets, which must be minimized within the feasible region. Since the level sets are concentric circles always centered at the origin, the cost function is determined solely by the radius. A larger radius corresponds to a higher cost. At any given radius, all points on the circle share the same cost, namely same $\|\boldsymbol{\tau}\|_2$, as shown in Fig.3.8a. If $\mathbf{0}$, center of the circular level set, is contained within $\mathbf{P}$, it represents the global minimum of the cost function, as, for example, in Fig. 3.2. Conversely, if the center lies outside the feasible region, the optimal solution is obtained by expanding the circle until it first intersects the feasible polygon. This intersection occurs either at a vertex or along an edge of the polygon, as illustrated in Fig. 3.3.

In contrast, the Quadratic Programming Parasitics (QPP) defines a cost function with elliptical level sets. Unlike QPT, where the cost function is determined solely by

[4] In the general formulation presented in Appendix A, the complementary slackness condition holds automatically due to the absence of inequality constraints.

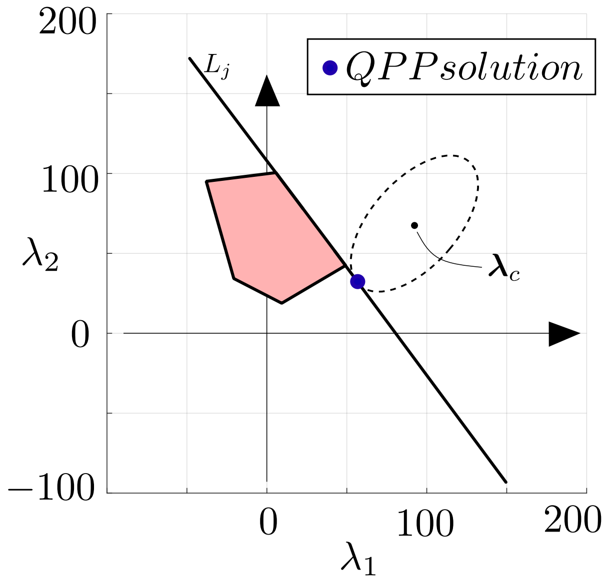

Figure 3.7: Example of QPP unfeasible edge search ($\boldsymbol{\lambda} \notin \mathbf{P}$) along inequality line L_j.

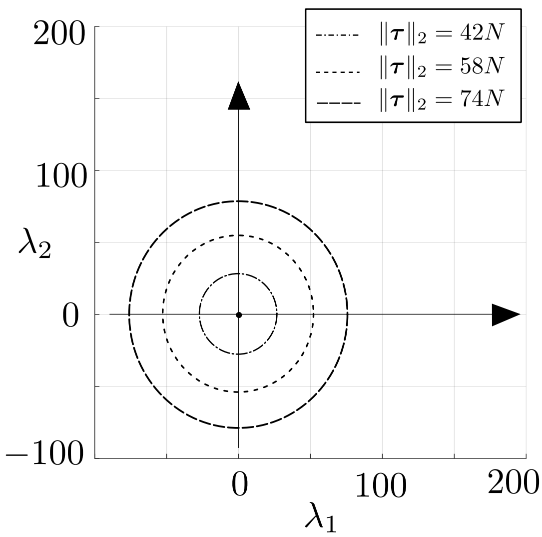

(a) Cost levels QPT: circles centered at the origin

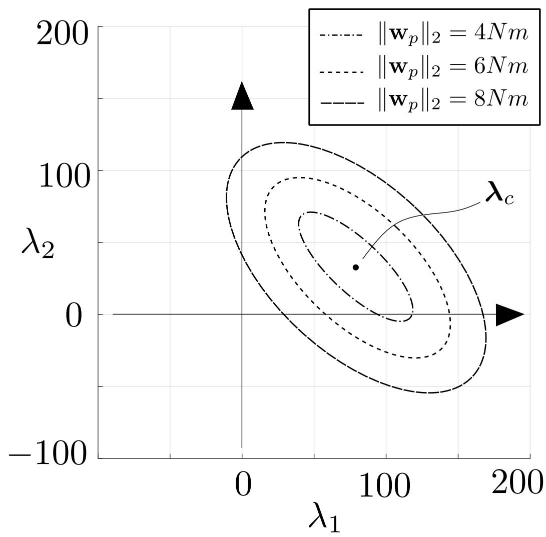

(b) Cost levels QPP: ellipses

Figure 3.8: Cost levels QPT and QPP.

the radius, the elliptical level sets of QPP depend on three parameters: the center, which determines the ellipse position, and the two semi-axes, which determine the ellipse shape. If the center of the elliptical level set in QPP lies within **P**, it represents the global minimum of the cost function, achieving the lowest possible cost (Fig. 3.5). When the center is outside the feasible region, the optimal solution is found by expanding the ellipse outward at higher and higher cost levels, as shown in Fig. 3.8b, until it first intersects the feasible polygon, occurring either at a vertex or along an edge, as for example happens in Fig. 3.6.

Through simulation, we observed that the presence of a linear term in the QPP cost function (3.10) can impact the continuity of its solutions over time. Specifically, changes in the end-effector (EE) pose can cause significant shifts in the center of the

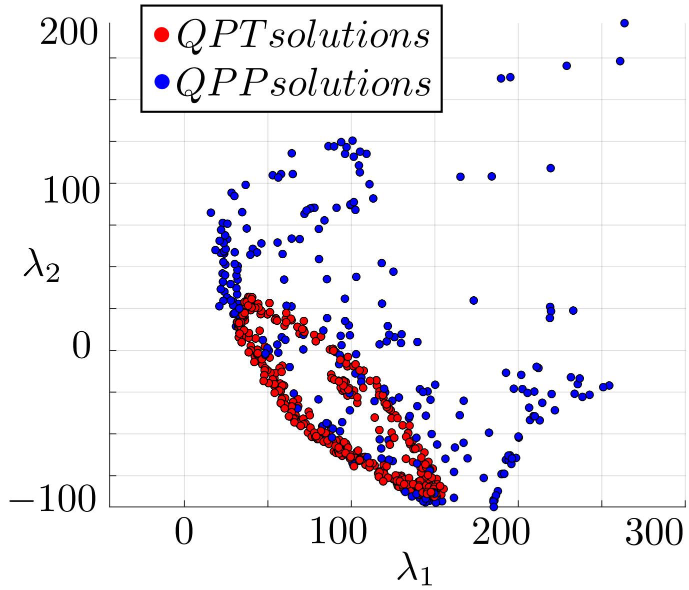

Figure 3.9: Comparison of $\boldsymbol{\lambda}$ solutions over time for QPT (red) and QPP (blue) with a simulated 4-cable CDWA: QPT solutions exhibit continuity and form a clear pattern, while QPP solutions are scattered, indicating potential discontinuities. The controlled wrench dimension is $m = 2$, with a null-space dimension of $n - m = 2$.

elliptical level sets due to the influence of the linear term. As a result, the computed values of $\boldsymbol{\lambda}$ may vary considerably between consecutive time steps. In particular, we could observe that the continuity of $\boldsymbol{\lambda}$ solutions over time is particularly sensitive to changes in EE orientation.

Conversely, in the absence of a linear term, the QPT cost function results in level sets that are concentric circles always centered at the origin. This inherent property prevents shifts in the center position over time, promoting greater continuity in the computed $\boldsymbol{\lambda}$ values. Consequently, the tension distribution remains smooth over consecutive time steps, avoiding abrupt variations, as previously reported in the literature [28].

Figure 3.9 illustrates the solutions of $\boldsymbol{\lambda}$ obtained using QPT (red markers) and QPP (blue markers) at each time step of a simulation conducted using real kinematic data from a 4-cable CDWA experiment. The controlled wrench $\mathbf{w}_c$ has a dimension $m = 2$, resulting in a null-space of dimension $n - m = 2$.

The QPT solutions exhibit continuity over time, forming a clear, continuous and well-defined pattern. In contrast, the QPP solutions are scattered without any discernible structure, highlighting the potential for discontinuities in the $\boldsymbol{\lambda}$ solutions provided by QPP.

However, the sensitivity of the QPT and QPP tension distribution to changes in EE position and orientation has not yet been systematically analyzed and remains an open question for future research.

Chapter 4

Performance Metrics for Cable-Driven Wrench Applicators

In this chapter, we introduce three new performance metrics for evaluating cable-driven wrench applicators (CDWAs). These metrics serve two primary objectives:

1. Evaluating tension distribution strategies for a given robot architecture using the *Overall Performance Index (OPI)*.

2. Comparing different robot architectures based on a fixed tension distribution using the *Maximum Parasitic-Wrench Index (MPI)* and the *Maximum Tension Index (MTI)*.

The proposed metrics are local, meaning they are computed for a specific position i and a set of relevant orientations. To provide a broader analysis, the workspace is discretized into N positions, each associated with M orientations. This allows the metrics to be evaluated both globally across the entire workspace and locally in task-relevant regions.

Additionally, as mentioned in Chapter 2, $\mathbf{w}_c$, $\mathbf{w}_r$ and $\mathbf{w}_p$ should be defined such that they contain either only forces or moments. This ensures dimensional consistency in the cost functions defined in Eqs. (3.5) and (3.9), as well as in the performance metrics.

To illustrate these concepts, we present examples based on a 4-cable CDWA architecture, where two wrench components are actively controlled while the remaining four components remain uncontrolled. This results in a null-space dimension of $r = n - m = 2$, allowing the analysis to be conducted in a 2D space of vectors $\boldsymbol{\lambda}$. This simplification enables intuitive geometric reasoning to better understand the performance evaluation framework.

4.1 Comparison of two tension distributions through OPI

The *Overall Performance Index* (OPI) is a dimensionless index developed to evaluate and compare the effectiveness of two tension distributions in a CDWA. Different tension distributions may require a trade-off between cable tensions (and consequently power, safety concerns, etc..) and parasitic wrench components that negatively impact the task. Determining $\boldsymbol{\lambda}$ with QPT minimizes cable tensions at the potential expense of higher parasitic components, whereas using QPP may do the opposite. This trade-off

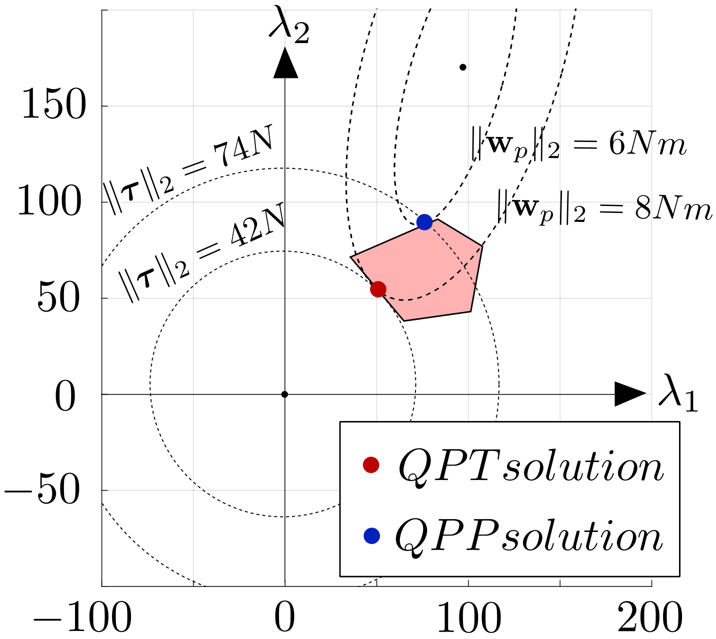

Figure 4.1: Example of a 2-D scenario where a trade-off between QPT and QPP is necessary.

is illustrated in Fig. 4.1, using the 2-D scenario introduced earlier (i.e., a 4 cable robot with $r = 2$).

In this example, we consider the parasitic wrench $\mathbf{w}_p$ comprising moments, i.e., $\mathbf{w}_p = [M_x \quad M_y \quad M_z]^\top$. Given a fixed end-effector (EE) pose, the feasible tension polygon $\mathbf{P}$ is computed using the method described in [27] (see Section 3.3.1) and is represented in pink in Fig. 4.1. The red marker denotes the solution obtained via QPT, which minimizes $\|\boldsymbol{\tau}\|_2$ and results in an optimal cable tension norm of $\|\boldsymbol{\tau}\|_2 = 42N$. In contrast, the blue marker corresponds to the QPP solution, which minimizes $\|\mathbf{w}_p\|_2$ and achieves an optimal parasitic moment norm of $\|\mathbf{w}_p\|_2 = 6Nm$.

From Fig. 4.1, it is evident that selecting the QPT solution (red marker) results in higher parasitic moments of $\|\mathbf{w}_p\|_2 = 8Nm$, whereas the QPP solution (blue marker) leads to a significantly higher cable tension norm of $\|\boldsymbol{\tau}\|_2 = 74N$. This demonstrates the necessity of a trade-off between different tension distributions, for example those given by QPT and QPP, to achieve a balanced performance.

The OPI serves as a quantitative tool to compare two alternative tension distributions and determine which one provides the most favorable compromise between minimizing cable tensions and reducing parasitic effects.

Given:

- an EE position
- a set of M task-relevant orientations
- two tension distributions, one computed by QPT (denoted by $\boldsymbol{\tau}_T$) and the other by QPP (denoted by $\boldsymbol{\tau}_P$)

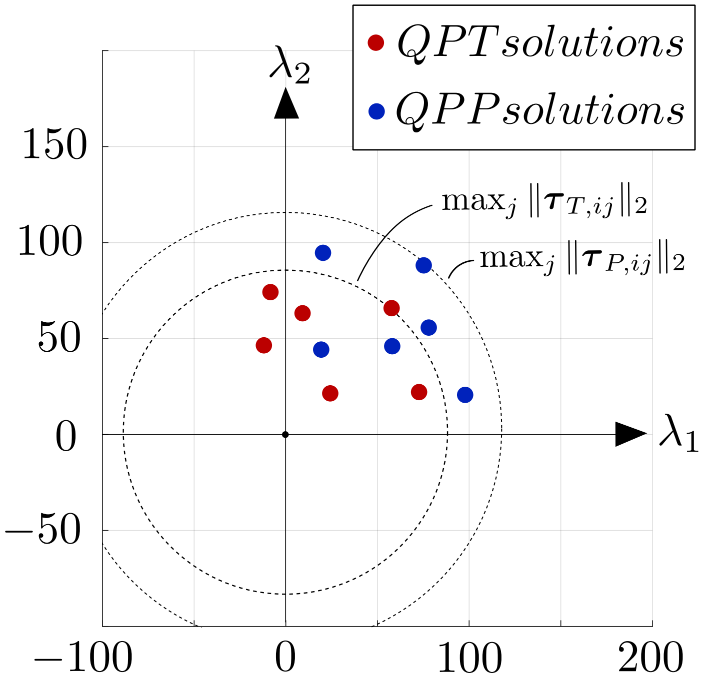

Figure 4.2: Geometric explanation in 2-D of $\boldsymbol{\tau}^*_{T,i}$ and $\boldsymbol{\tau}^*_{P,i}$. In red, different $\|\boldsymbol{\tau}_T\|_2$ provided by QPT, in blue, different $\|\boldsymbol{\tau}_P\|_2$ provided by QPP, computed over the M orientations, at a fixed EE position i.

we define:

$$\boldsymbol{\tau}^*_{T,i} = \max_j \frac{\|\boldsymbol{\tau}_{T,ij}\|}{\sqrt{n}}, \qquad \boldsymbol{\tau}^*_{P,i} = \max_j \frac{\|\boldsymbol{\tau}_{P,ij}\|}{\sqrt{n}} \tag{4.1}$$

$$\mathbf{w}^*_{p_{T,i}} = \max_j \|\mathbf{w}_{p_{T,ij}}\|, \qquad \mathbf{w}^*_{p_{P,i}} = \max_j \|\mathbf{w}_{p_{P,ij}}\| \tag{4.2}$$

where j is the index that identifies a specific orientation in the list of the considered ones, with $j = 1, \ldots, M$. Basically, $\boldsymbol{\tau}^*_{T,i}$ and $\boldsymbol{\tau}^*_{P,i}$ are the largest RMS values of the tension arrays among the considered orientations, computed with QPT and QPP, respectively. Similarly, $\mathbf{w}^*_{p_{T,i}}$ and $\mathbf{w}^*_{p_{P,i}}$ represent the largest 2-norm values of the parasitic wrench among the considered orientations.

In a robot with $n = m+2$ cables, the norm $\|\boldsymbol{\tau}\|_2$ describes a circle centered at $\boldsymbol{\lambda} = \mathbf{0}$, allowing for a straightforward geometric interpretation of the terms $\boldsymbol{\tau}^*_{T,i} = \max_j \|\boldsymbol{\tau}_{T,ij}\|/\sqrt{n}$ and $\boldsymbol{\tau}^*_{P,i} = \max_j \|\boldsymbol{\tau}_{P,ij}\|/\sqrt{n}$. These quantities can be visualized by solving the QPT and QPP formulations across M different orientations, where the solutions obtained from QPT and QPP are represented as red and blue markers, respectively. Neglecting, for the moment, the scaling factor $\sqrt{n}$ appearing in (4.1), the term $\boldsymbol{\tau}^*_{T,i}$ corresponds to the minimum-radius circle that encloses all red markers, while $\boldsymbol{\tau}^*_{P,i}$ is defined analogously for the blue markers. This geometric representation is illustrated in Fig. 4.2, which depicts the distribution of $\|\boldsymbol{\tau}_T\|_2$ and $\|\boldsymbol{\tau}_P\|_2$ over multiple orientations at a fixed end-effector position i. A similar geometric representation cannot be applied to $\mathbf{w}^*_{p_{T,i}}$ and $\mathbf{w}^*_{p_{P,i}}$, as different orientations provide changes in both position and shape of the corresponding ellipses, and the spatial relationship between a marker's position in the $\boldsymbol{\lambda}$

space and its associated $\|\mathbf{w}_p\|$ is no longer preserved, making a direct visualization of these quantities not straightforward.

The *Overall Performance Index* (OPI) at position i is defined as:

$$\mathrm{OPI}_i = \Delta\boldsymbol{\tau}_i + \Delta\mathbf{w}_{p,i} \tag{4.3}$$

where

$$\Delta\boldsymbol{\tau}_i = \frac{\boldsymbol{\tau}^*_{\mathrm{P},i} - \boldsymbol{\tau}^*_{\mathrm{T},i}}{(\boldsymbol{\tau}^*_{\mathrm{P},i} + \boldsymbol{\tau}^*_{\mathrm{T},i})/2} \cdot 100, \quad \Delta\mathbf{w}_{p,i} = \frac{\mathbf{w}^*_{p_{\mathrm{P},i}} - \mathbf{w}^*_{p_{\mathrm{T},i}}}{(\mathbf{w}^*_{p_{\mathrm{P},i}} + \mathbf{w}^*_{p_{\mathrm{T},i}})/2} \cdot 100. \tag{4.4}$$

Here:

- $\Delta\boldsymbol{\tau}_i$ quantifies the relative change in cable tensions, with respect to the mean value, when switching from QPT to QPP.
- $\Delta\mathbf{w}_{p,i}$ quantifies the relative change in parasitic components, with respect to the mean value, under the same transition.

Since strictly convex quadratic optimization problems have a unique global solution [27], at each j-th orientation the solution found by QPT is certainly the global optimum for $\|\boldsymbol{\tau}\|_2$, while the one found by QPP is certainly the global optimum for $\|\mathbf{w}_p\|$. This holds:

$$\boldsymbol{\tau}^*_{\mathrm{T},i} \le \boldsymbol{\tau}^*_{\mathrm{P},i}, \quad \mathbf{w}^*_{p_{\mathrm{P},i}} \le \mathbf{w}^*_{p_{\mathrm{T},i}}. \tag{4.5}$$

From Eqs. (4.2), the denominators in Eqs. (4.4) are always positive. Additionally, the conditions established in Eqs. (4.5) ensure that the numerator of $\Delta\boldsymbol{\tau}_i$ is positive, while the numerator of $\Delta\mathbf{w}_{p,i}$ is negative. As a result, we obtain:

$$\Delta\boldsymbol{\tau}_i \ge 0, \quad \Delta\mathbf{w}_{p,i} \le 0 \tag{4.6}$$

A positive OPI indicates that the reduction achieved by QPP in parasitic components ($\Delta\mathbf{w}_{p,i} \le 0$) cannot outweigh the increase in cable tensions ($\Delta\boldsymbol{\tau}_i \ge 0$), favoring the use of QPT overall. The opposite happens when OPI is negative. Thus, when OPI is *greater than* 0, QPT is more advantageous, while having an OPI *smaller than* 0 suggests the opposite. OPI is *equal to* 0 if $\boldsymbol{\tau}^*_{\mathrm{T},i} = \boldsymbol{\tau}^*_{\mathrm{P},i}$ and $\mathbf{w}^*_{p_{\mathrm{P},i}} = \mathbf{w}^*_{p_{\mathrm{T},i}}$, meaning that Eqs.(4.1) and (4.2) selected, across the different orientations, a tension distribution and a parasitic wrench which encapsule the same $\boldsymbol{\lambda}$, resulting in QPT coinciding with QPP.

The definition of $\Delta\boldsymbol{\tau}_i$ and $\Delta\mathbf{w}_{p,i}$ presented earlier assume that OPI were computed to evaluate the transition from QPT to QPP. However, if OPI was instead computed by comparing QPP against QPT, the expressions for $\Delta\boldsymbol{\tau}_i$ and $\Delta\mathbf{w}_{p,i}$ would be reversed as follows:

$$\Delta\boldsymbol{\tau}_i = \frac{\boldsymbol{\tau}^*_{\mathrm{T},i} - \boldsymbol{\tau}^*_{\mathrm{P},i}}{(\boldsymbol{\tau}^*_{\mathrm{T},i} + \boldsymbol{\tau}^*_{\mathrm{P},i})/2} \cdot 100, \quad \Delta\mathbf{w}_{p,i} = \frac{\mathbf{w}^*_{p_{\mathrm{T},i}} - \mathbf{w}^*_{p_{\mathrm{P},i}}}{(\mathbf{w}^*_{p_{\mathrm{T},i}} + \mathbf{w}^*_{p_{\mathrm{P},i}})/2} \cdot 100. \tag{4.7}$$

Despite this change in formulation, the interpretation of OPI remains unchanged: an OPI *greater than* 0 still indicates the the original method (previously QPT, now QPP) is preferable, while OPI *smaller than* 0 suggests the opposite.

The OPI index has some drawbacks that should be considered. By directly summing the two contributions of $\Delta\boldsymbol{\tau}_i$ and $\Delta\mathbf{w}_{p,i}$ without weighting them, we implicitly assume that the two terms have the same importance. Depending on the application, though, this might not be true, and weighting the two factors may be relevant. Moreover, when both $\mathbf{w}^*_{p_{\mathrm{P},i}}$ and $\mathbf{w}^*_{p_{\mathrm{T},i}}$ are close to zero (which is an ideal situation), $\Delta\mathbf{w}_{p,i}$ may become undefined. A possible solution could be to define a threshold such that, when both terms in $\Delta \mathbf{w}_{p,i}$ are very small, $\mathbf{w}_{p,i}$ is set to zero. In this case, OPI only depends on $\boldsymbol{\tau}$, since $\mathbf{w}_p$ is ideal in both optimizations.

By analyzing OPI across the workspace, it is possible to identify regions that suggest the use of specific tension distribution, as their advantages outweigh disadvantages. Therefore, OPI provides a practical tool for selecting which tension distribution should be used among two potential candidates, either across the entire workspace or within specific regions relevant to the task. By identifying tension distributions that optimally balance tensions and parasitic wrench-components, OPI contributes to strengthening the performance of CDWAs. An example of OPI application is provided in Chapter 5.

4.2 Comparison of different robot architectures through MTI and MPI

The *Maximum Tension Index* (MTI) and *Maximum Parasitic-Wrench Index* (MPI) are designed to evaluate the performance of different CDWAs, as they provide a measure of the system's ability to work with minimal effort (thus, minimizing cable tensions) and limited interference to the task (thus, minimizing the parasitic effects), once a tension distribution strategy is selected.

Given an EE position i, and its set of M task-relevant orientations, the MTI and MPI are defined as:

$$\mathrm{MTI}_i = \max_j \|\boldsymbol{\tau}_{ij}\|/\sqrt{n}, \qquad \mathrm{MPI}_i = \max_j \|\mathbf{w}_{p,ij}\| \tag{4.8}$$

The MTI_i measures the maximum RMS value of the tension array at position i, and MPI_i measures the maximum 2-norm of the parasitic wrench, across M different orientations. For the MTI_i it is possible to make similar consideration as in the previous section. In a robot with $n = m+2$ cables, the norm $\|\boldsymbol{\tau}\|_2$ describes a circle centered at $\boldsymbol{\lambda} = \mathbf{0}$, allowing for a geometric interpretation of the MTI_i. By finding cable tensions with the previously selected tension distribution across M different orientations, and neglecting, for the moment, the scaling factor $\sqrt{n}$, the term MTI_i corresponds to the minimum-radius circle that encloses all black markers. This geometric representation is illustrated in Fig. 4.3, which depicts the distribution of $\|\boldsymbol{\tau}\|_2$ over multiple orientations at a fixed end-effector position i. Similarly to the previous section, geometric representation cannot be applied to the MPI_i, as different orientations provide changes in both position and shape of the corresponding ellipses. Consequently, the spatial relationship between a marker's position in the $\boldsymbol{\lambda}$ space and its associated $\|\mathbf{w}_p\|$ would no longer preserved, making a direct visualization of these quantities infeasible.

The workspace can be mapped with MTI and MPI values, enabling a quantitative assessment of the robot performance. These indices can be useful for:

- identifying regions within the workspace where the robot experiences high cable tensions or parasitic effects.
- designing tasks by selecting trajectories that pass through areas with low MTI and MPI values.
- comparing different robot architectures under the same workspace and task constraints.

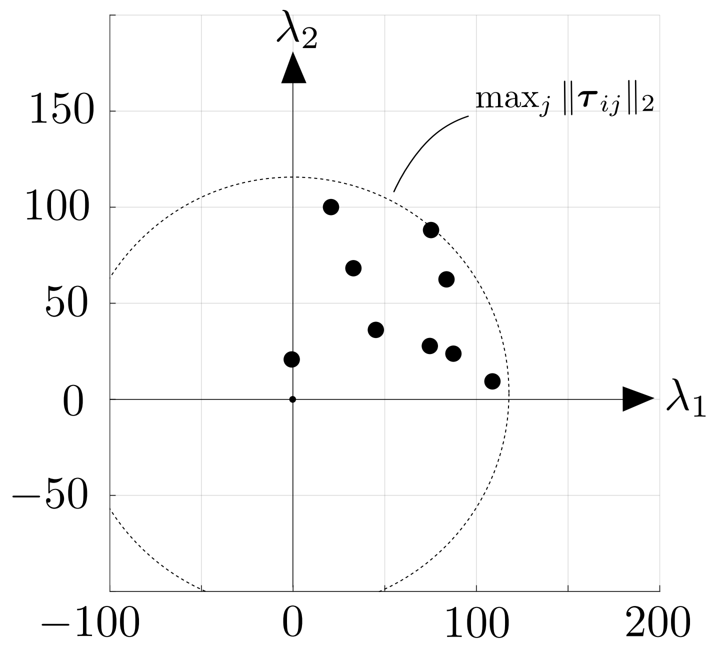

Figure 4.3: Geometric explanation in 2-D of the MTI_i. In black, different values of norm $\|\boldsymbol{\tau}\|_2$ computed over the M orientations, at a fixed EE position i.

The MTI and MPI may serve as tools for evaluating and optimizing CDWAs, facilitating informed design and task decisions.

4.3 Collective framework to analyze and compare CDWAs

The Overall Performance Index (OPI), Maximum Tension Index (MTI), and Maximum Parasitic-Wrench Index (MPI) together form a structured framework for evaluating Cable-Driven Wrench Applicators (CDWAs). These indices are intended to be used in a sequential manner to systematically assess different aspects of performance.

First, the OPI is used to determine the most suitable tension distribution (TD) strategy by evaluating how different TD choices affect overall performance. Once the optimal TD is selected, MTI and MPI are employed to compare performance across different robot architectures or task conditions. Specifically, these indices allow for the evaluation of different CDWA designs performing the same task, the same CDWA executing different tasks, and various actuation strategies applied to the same device. This layered approach ensures that the evaluation process accounts for both task-dependent optimization and hardware-dependent performance variations.

The structured nature of this framework enables direct comparisons between different cable-driven systems, regardless of their design complexity or degree of actuation redundancy. By analyzing key performance factors in a systematic manner, it provides a standardized methodology for assessing tension distribution strategies and performance (cable tensions and undesired parasitic wrenches) in applications such as rehabilitation robotics, assistive exoskeletons, and force-feedback devices.

Beyond its role in performance assessment, this framework can be applied to design, optimization and task-specific tuning. By analyzing how each index varies under different task conditions, cable configurations, and control strategies, engineers can identify design trade-offs, improve system efficiency, and enhance overall functionality. The following Chapter illustrates how this framework was applied to evaluate the performance of 4-cable and 8-cable CDWAs executing the same rehabilitation task. Through this analysis, the two configurations were systematically compared, leading to the validation that, for this specific task, the 8-cable device could be effectively replaced by a simpler and more cost-efficient 4-cable alternative without compromising performance.

Chapter 5

Framework Application: Comparison of Two Cable Driven Wrench Applicators for Rehabilitation

This chapter applies the proposed framework to analyze and compare Cable-Driven Wrench Applicators (CDWAs) for rehabilitation. Specifically, we focus on a subset of these systems known as *Cable-Driven Force Applicators* (CDFAs), where forces must be precisely controlled while minimizing unwanted parasitic moments. Accurate force application is essential in rehabilitation, as controlled forces facilitate effective patient training, whereas undesired moments may introduce instability or discomfort [34].

The goal of this study is to evaluate whether a simpler, more accessible, and cost-effective 4-cable CDFA can effectively replace an 8-cable system for a specific rehabilitation task. While 8-cable systems offer enhanced control over applied forces and moments, they come with added complexity, increased costs, and potential usability challenges, which may hinder their adoption in clinical settings. The core trade-off explored in this chapter is between system complexity, accessibility, and performance.

This research is motivated by the need to increase accessibility for physiotherapists during rehabilitation tasks. The ROAR Lab at Columbia University works with spinal cord injury (SCI) patients, who often require continuous hands-on intervention from clinicians while using robotic assistance. However, in an 8-cable system, the physical constraints imposed by multiple cables can limit real-time therapist interaction, making the therapy less practical and efficient. In contrast, a 4-cable system reduces obstructions, allowing for easier patient access and a more natural therapist-patient interaction during training.

The focus of this study is to determine whether a 4-cable CDFA, which offers greater accessibility and ease of use, can effectively perform the same rehabilitation task as an 8-cable system while maintaining high performance in force application.

Demonstrating the feasibility of a 4-cable system would highlight its potential to reduce complexity and improve accessibility in clinical environments, thereby facilitating the adoption of CDWAs in rehabilitation settings. A system with fewer cables could provide a simpler yet effective rehabilitation solution while maintaining therapeutic efficacy and ensuring a practical balance between performance and usability.

To systematically compare these two devices, we employ the proposed framework, which consists of three key components:

1. *Tension distribution selection using the Overall Performance Index (OPI):* Ensures

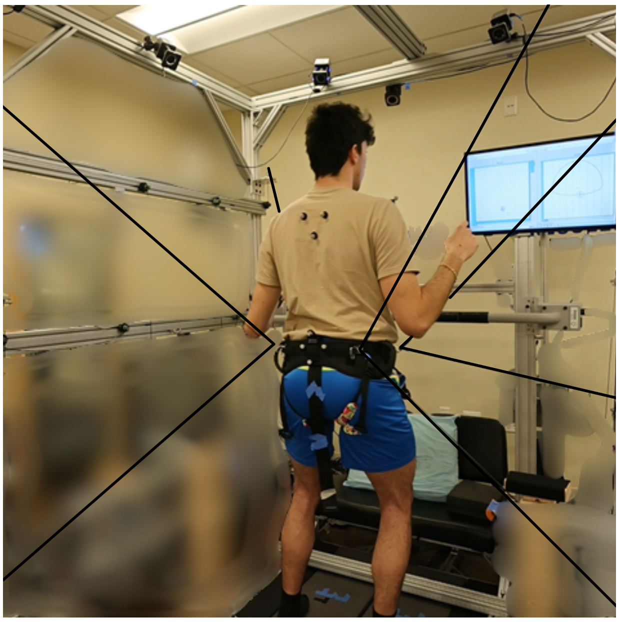

Figure 5.1: Exercise setup: a pelvic belt is attached to 8 cables while a screen in front of the patient displays the trajectory to be followed.

that the cable-generated forces achieve the desired wrench while minimizing cable tensions and reducing parasitic effects.

2. *Performance evaluation using the Maximum Tension Index (MTI) and Maximum Parasitic-Wrench Index (MPI):* Quantifies how well each system transmits the desired forces while minimizing cable tensions and undesired moments.

3. *Experimental validation:* Verifies the practical feasibility of the framework's predictions using real experimental data.

By structuring the comparison in this way, we aim to provide an objective and systematic evaluation of 4-cable vs 8-cable CDFAs, highlighting their respective advantages and limitations in the rehabilitation context. The results will offer insights into whether simpler systems can achieve comparable performance to more complex alternatives, and what trade-offs arise in terms of force accuracy and patient experience.

Beyond the specific case of these two systems, this analysis demonstrates the broader applicability of the proposed CDWA evaluation framework. The methodology developed in this study can be generalized to compare other cable-driven devices, helping guide future design choices in rehabilitation robotics.

5.1 Rehabilitation task and system setup

The rehabilitation task is designed to enhance stand-balance capabilities by challenging the patient's stability in a controlled manner. During the session, the patient stands with their feet in a fixed position while wearing a pelvic belt, which serves as the robot's end-effector (EE). The patient is instructed to follow a custom-designed trajectory displayed on a screen in front of them (Fig. 5.1).

The task consists of two main phases:

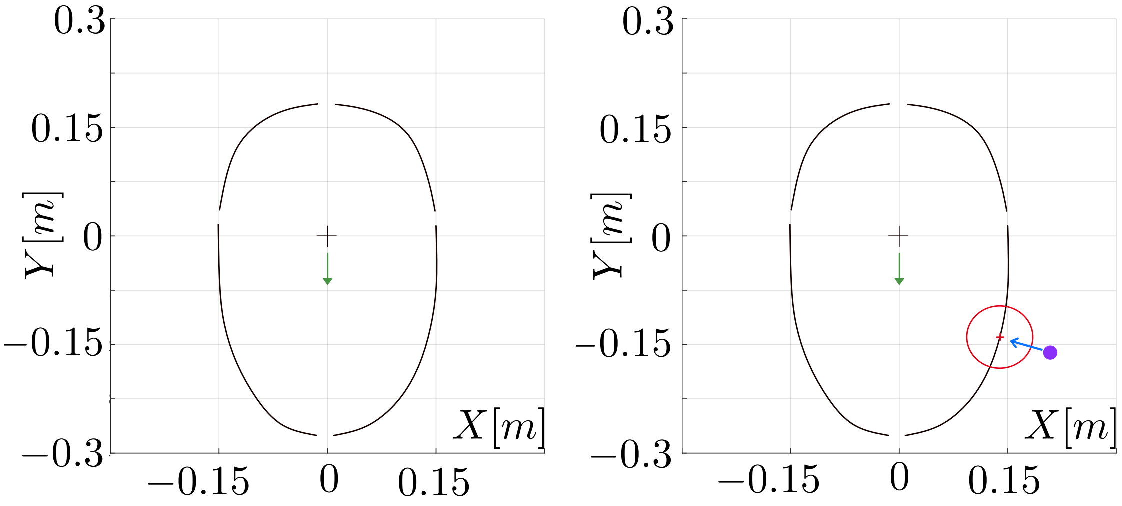

(a) Example of a customized trajectory that the patient is required to follow with their center of mass. The green arrow indicates the direction the patient is facing during training.

(b) Force field in red, COM instantaneous position in purple and desired assistive force in blue.

Figure 5.2: Task trajectory and force field.

1. *Offline Base of Support (BOS) Assessment*: before the training session begins, the patient's Base of Support (BOS) is evaluated using the *Star Reaching Test* [35]. This test allows for an individualized assessment of the patient's stability limits and is used to design a custom trajectory that effectively challenges their equilibrium.

2. *Online Robot-Assisted Training*: during training, the patient is required to shift their center of mass (COM) along the predefined trajectory (Fig. 5.2a). This involves controlled bending movements to reach different positions while maintaining balance.

To ensure patient safety and assist only when necessary, the robot employs an assist-as-needed control strategy [36]. Specifically, when the real-time COM position deviates from the trajectory by more than the force field radius, the robot applies planar horizontal assistive forces F_x, F_y, equal to 10% of the patient's body weight, directed towards the center of the force field (Fig. 5.2b. This assistance is intended to guide the patient back towards stability without overcompensating.

The task is currently implemented using the RobUST robot [37], which features an 8-cable design (Fig. 5.1). The robot's geometric configuration has been reconstructed in Fig. 5.4a, with detailed geometric parameters provided in Tab. 5.1. The COM position is continuously tracked in real time using a Vicon motion capture system, which consists of high-speed cameras capturing reflective marker positions at a sampling frequency of 200 Hz (Fig. 5.3). These markers, strategically placed on both the robot's EE and the patient, enable high-precision kinematic tracking, eliminating the need to solve the analytical forward geometric problem (2.1.1).

In this study, we applied the presented framework to evaluate the feasibility of a simplified 4-cable design (Fig.5.4b, geometric parameters in Tab. 5.2), with all pulleys positioned in a single intermediate plane, to improve accessibility for the physiotherapist during the rehabilitation task, while maintaining adequate performance.

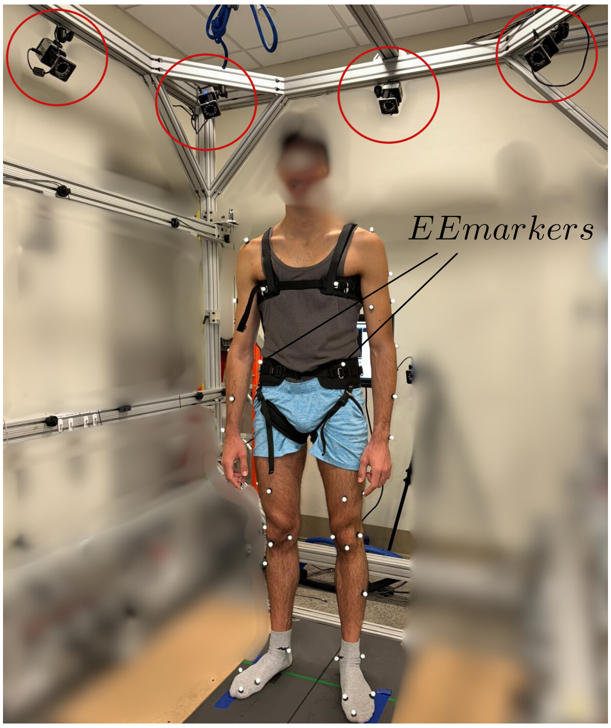

Figure 5.3: Vicon motion capture system: cameras (circled in red) and markers. Markers on the EE are for kinematic tracking, while those on the human body are for biomechanical analysis.

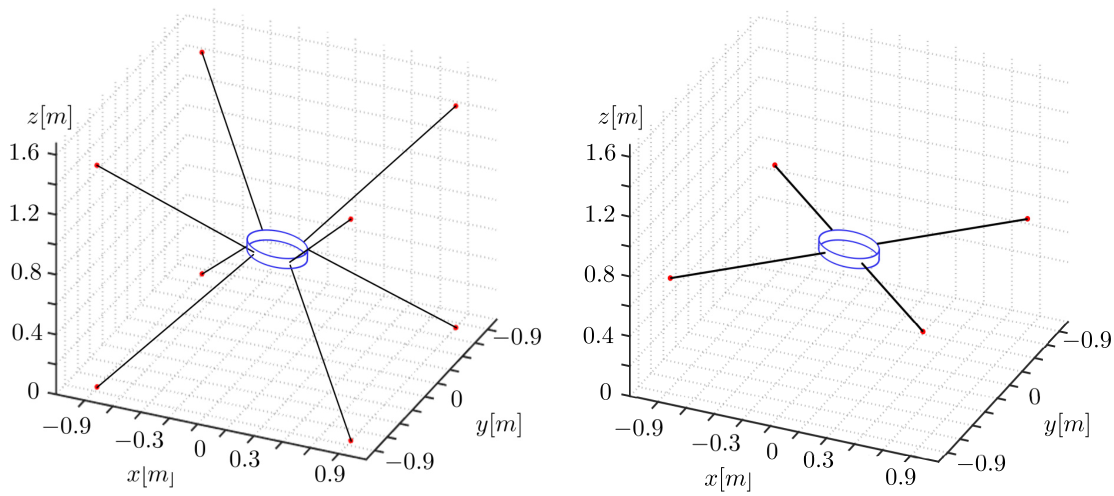

(a) 8-cables CDFA (RobUST).

(b) 4-cables CDFA.

Figure 5.4: Architecture comparison: CDWAs eyelets are in red, cables are black lines, and the cylindrical object is the EE.

The volume relevant to the rehabilitation exercise was discretized, in both architectures, with $N = 1000$ positions and a set of $M = 15$ orientations for each position, as shown in Fig.5.5. The workspace bounds were set to $x, y \in [-0.5, 0.5]\,m$ and $z \in [0.3, 1.2]\,m$ for position, and $\pm 20°$ (tilt) and $\pm 10°$ (torsion) for orientation, as suggested in [38]. The patient's body weight was considered to be 85 kg, and the desired wrench 10% of this body weight, to be applied at the center of mass of the EE. Two tension

Table 5.1: Geometrical parameters of the RobUST architecture.

i	1	2	3	4	5	6	7	8
$\mathbf{b}_i$ [m]	$\begin{bmatrix}0.9\\-0.9\\0\end{bmatrix}$	$\begin{bmatrix}0.9\\0.9\\0\end{bmatrix}$	$\begin{bmatrix}-0.9\\-0.9\\0\end{bmatrix}$	$\begin{bmatrix}-0.9\\0.9\\0\end{bmatrix}$	$\begin{bmatrix}0.9\\-0.9\\1.5\end{bmatrix}$	$\begin{bmatrix}0.9\\0.9\\1.5\end{bmatrix}$	$\begin{bmatrix}-0.9\\-0.9\\1.5\end{bmatrix}$	$\begin{bmatrix}-0.9\\0.9\\1.5\end{bmatrix}$
$\mathbf{r}'_i$ [m]	$\begin{bmatrix}0.14\\-0.14\\-0.05\end{bmatrix}$	$\begin{bmatrix}0.14\\0.14\\-0.05\end{bmatrix}$	$\begin{bmatrix}-0.14\\-0.14\\-0.05\end{bmatrix}$	$\begin{bmatrix}-0.14\\0.14\\-0.05\end{bmatrix}$	$\begin{bmatrix}0.14\\-0.14\\0.05\end{bmatrix}$	$\begin{bmatrix}0.14\\0.14\\0.05\end{bmatrix}$	$\begin{bmatrix}-0.14\\-0.14\\0.05\end{bmatrix}$	$\begin{bmatrix}-0.14\\0.14\\0.05\end{bmatrix}$

Table 5.2: Geometrical parameters of the 4-cable architecture.

i	1	2	3	4
$\mathbf{b}_i$ [m]	$\begin{bmatrix}0.9\\-0.9\\0.75\end{bmatrix}$	$\begin{bmatrix}0.9\\0.9\\0.75\end{bmatrix}$	$\begin{bmatrix}-0.9\\-0.9\\0.75\end{bmatrix}$	$\begin{bmatrix}-0.9\\0.9\\0.75\end{bmatrix}$
$\mathbf{r}'_i$ [m]	$\begin{bmatrix}0.14\\-0.14\\0\end{bmatrix}$	$\begin{bmatrix}0.14\\0.14\\0\end{bmatrix}$	$\begin{bmatrix}-0.14\\-0.14\\0\end{bmatrix}$	$\begin{bmatrix}-0.14\\0.14\\0\end{bmatrix}$

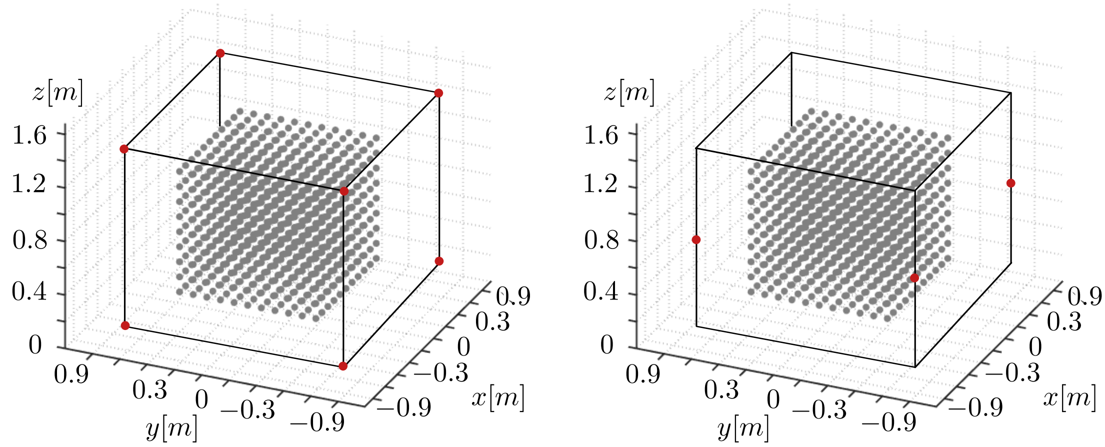

(a) 8-cables CDFA (RobUST). (b) 4-cables CDFA.

Figure 5.5: Discretized workspace: robot frame in black, cable eyelets in red, discrete workspace points in grey.

distributions, namely QPT and QPP, were compared for each architecture, and the following constraints were considered: $\tau_{\min} = 10\,\mathrm{N}$, $\tau_{\max} = 90\,\mathrm{N}$, $w_{r,\max} = 70\,\mathrm{N}$ (accounting for F_z), and $w_{p,\max} = 15\,\mathrm{Nm}$ (accounting for parasitic moments M_x, M_y, M_z). The mathematical framework described in Chapter 3 was implemented for both architectures in MATLAB. (3.8) and (3.11) were solved by using the *quadprog* function, allowing for the computation of OPI, MTI, and MPI.

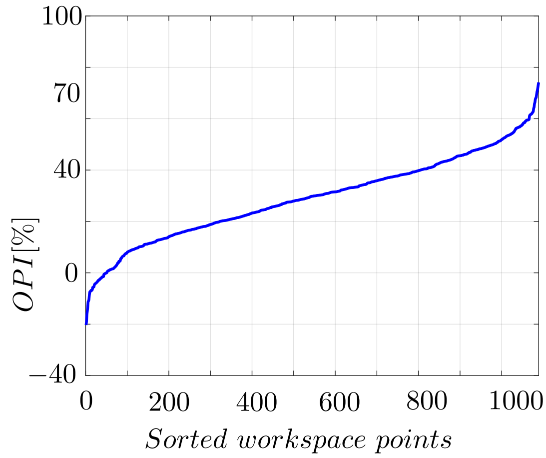

(a) 8-cable

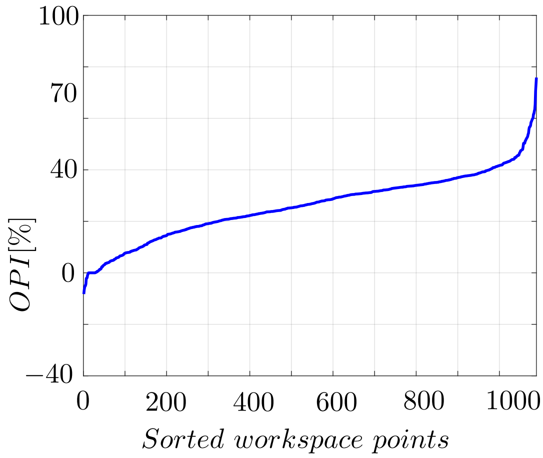

(b) 4-cable

Figure 5.6: OPI distribution over the workspace.

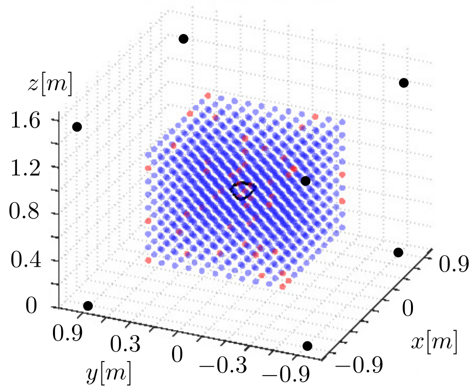

(a) Workspace and task trajectory

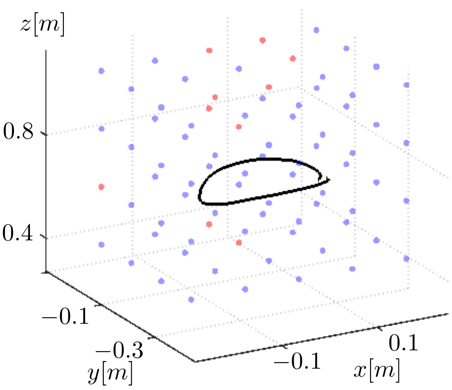

(b) Focus on task trajectory

Figure 5.7: Task subregion analysis of the 8-cable robot: task trajectory in black, positive OPI values in blue, negative OPI values in red.

5.2 Tension distribution selection through OPI

The comparison between tension distributions provided by QPT and QPP was evaluated through OPI for each robotic architecture, with the results illustrated in Fig. 5.6. In general, both 4-cable and 8-cable robots exhibit predominantly positive OPI values across the workspace, indicating the convenience of using QPT for both architectures. However, a notable subregion of the 8-cable robot's workspace (Fig. 5.6a) displays negative OPI values and requires further investigation.

To better assess the significance of these negative OPI values, we analyzed the intersection between a potential task's trajectory and the 3D workspace, as shown in Fig. 5.7. In this figure, the task trajectory (depicted in blue) is overlaid on a 3D map of OPI values. Blue dots represent points with positive OPI, while red dots indicate negative OPI values. As Fig. 5.7b demonstrates, the majority of the points surrounding the trajectory's relevant subregion are blue, suggesting that negative OPI values have minimal impact on the task. Therefore, QPT remains a viable and recommended choice even for the 8-cable device.

5.3 Performance evaluation through MTI and MPI

With the selected tension distribution (QPT) applied to both architectures, performance was analyzed in terms of cable tensions and parasitic moments, captured by MTI and MPI, respectively.

The 4-cable architecture demonstrates high MTI values, indicating significant cable tensions across the entire workspace, as shown in Fig. 5.8a, compared to the 8-cable architecture, which achieves consistently lower MTI values (Fig. 5.9a). Hence, for the given setup, the 8-cable system is more effective at minimizing cable tensions. Both architectures exhibit strong continuity in MTI values across adjacent positions, aligning well with the requirements in rehabilitation applications.

Regarding parasitic moments, the 4-cable configuration exhibits a steep gradient (Fig. 5.8b), with MPI values increasing substantially as positions move further away from the pulley plane. On the other hand, the 8-cable architecture displays a more uniform distribution of parasitic moments (Fig. 5.9b), maintaining relatively constant and generally higher values throughout the workspace.

For the rehabilitation task under consideration, the trajectory is positioned at the center of the workspace (Fig. 5.7), a region where the parasitic moments for the 4-cable architecture not only are significantly reduced, aligning well with the task's requirements. This localized reduction mitigates the impact of the 4-cable system's limitations and suggests that it can perform adequately for the given exercise.

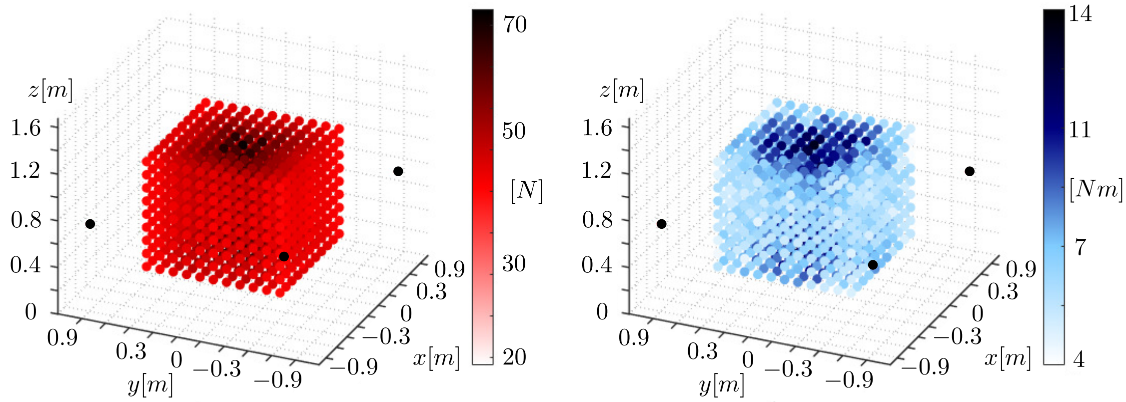

(a) 4-cable MTI

(b) 4-cable MPI

Figure 5.8: 4-cable performance.

5.4 Experimental validation

To validate the proposed framework and assess the feasibility of replacing an 8-cable CDWA with a more accessible 4-cable system, we conducted a controlled experimental study replicating the conditions used in simulation, described in Section 5.1. The experiment was designed to verify the predictions made by the framework regarding tension distribution and parasitic wrenches during a rehabilitation task.

A human subject was recruited to perform the same task under two different conditions: once with the 4-cable system and once with the 8-cable system. The experimental setup was carefully designed to match the simulated conditions as closely as

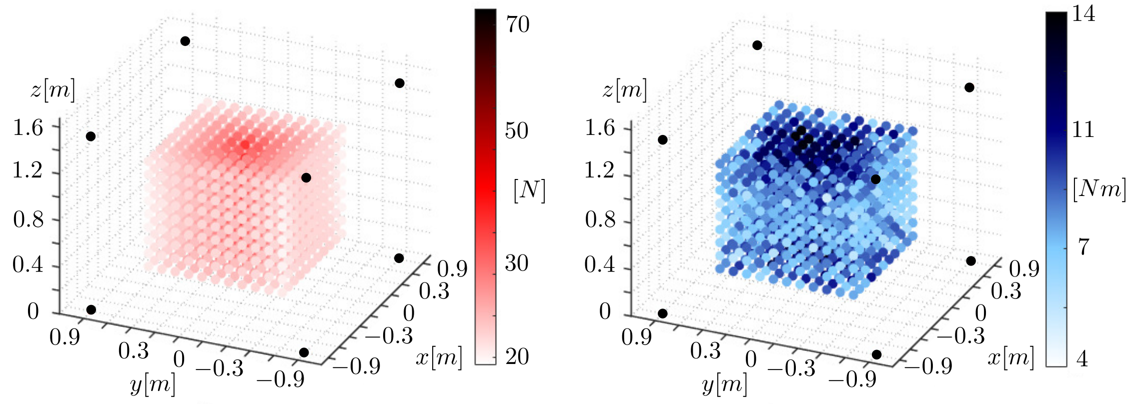

(a) 8-cable MTI (b) 8-cable MPI

Figure 5.9: 8-cable performance.

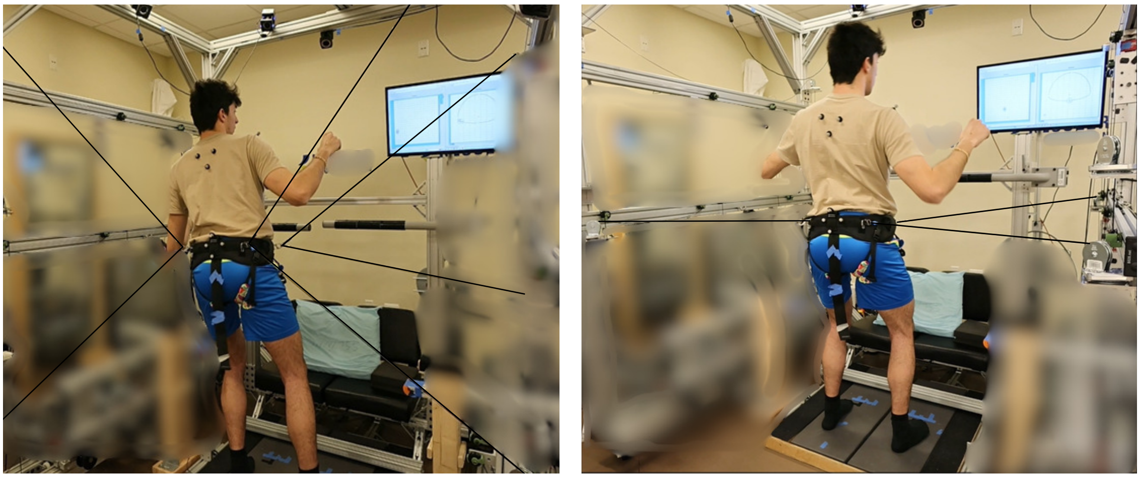

(a) 8-Cable robot (RobUST) (b) 4-cable robot

Figure 5.10: Experimental setup.

possible 5.10. The tension distribution for both configurations was determined using Quadratic Programming Tension (QPT) optimization, as recommended by the Overall Performance Index (OPI)(Section 5.2). The task parameters remained unchanged across both experiments to ensure a direct comparison.

During the trials, real-time data were collected on the end-effector (EE) trajectory, cable tensions, and structure matrices. The EE trajectory and the structure matrices were tracked using motion capture system, while load cell measurements provided direct recordings of the cable tensions. Fig.5.11 shows the EE trajectory in the 8-cable and 4-cable system, respectively.

The experimental results closely aligned with the theoretical predictions, validating the proposed framework. In terms of cable tensions (Fig.5.12), the 4-cable system exhibited consistently higher mean cable tensions compared to the 8-cable system, with a mean range of $35N$ to $45N$, whereas the 8-cable system showed lower mean tensions, ranging from $18N$ to $30N$. Additionally, the standard deviation of cable tensions was significantly larger in the 4-cable system (up to $50N$) compared to the 8-cable system (up to $25N$). These results indicate that, for this specific task and configuration, the reduction in the number of cables led to higher tension requirements to achieve the

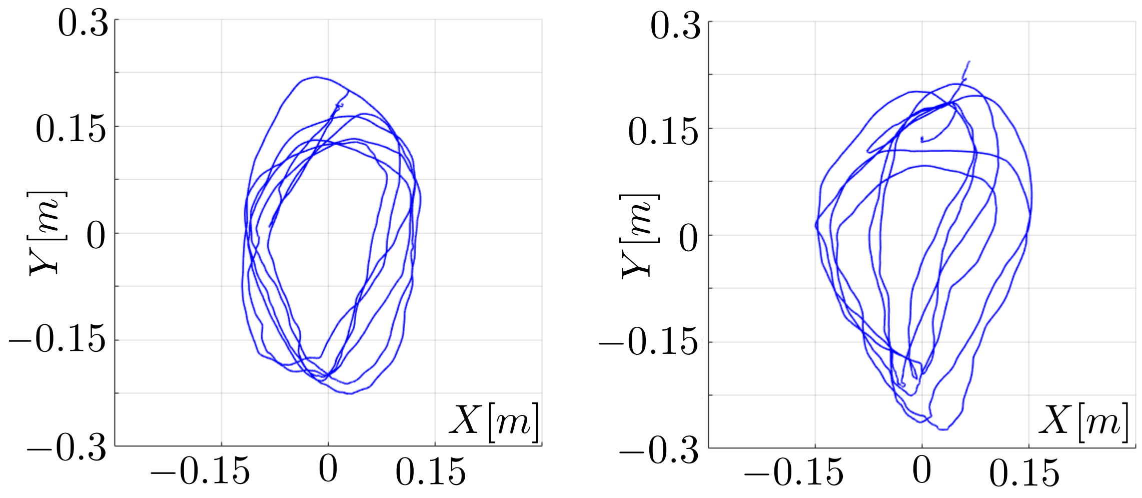

(a) 8-Cable robot (RobUST) (b) 4-cable robot

Figure 5.11: 2-D trajectories described by the belt centroid during the experiments. The exercise was repeated 6 times for each configuration, resulting in overlapping plots.

desired force application, aligning with predictions.

The parasitic moment analysis demonstrated a clear advantage for the 4-cable system in minimizing unwanted moments for this specific rehabilitation task and cable arrangement(Fig.5.13). While M_x values were comparable between the two configurations (mean of $3.7Nm$ for the 4-cable vs. $3.0Nm$ for the 8-cable system), the 4-cable system exhibited significantly lower parasitic effects in M_y and M_z. Specifically, the mean parasitic moment in M_y was approximately $1.5Nm$ for the 4-cable system compared to $5.0Nm$ in the 8-cable system, with a standard deviation nearly twice as large in the latter. The most striking difference was observed in M_z, where the 8-cable configuration exhibited a mean of $7.5Nm$, nearly *four times higher* than the $2.0Nm$ recorded for the 4-cable system. This confirms that, under the conditions of this specific example, reducing the number of cables leads to a more stable and controlled force application, effectively mitigating excessive parasitic moments.

Despite the increased cable tensions, which might contribute to a stiffer feel and potentially increased jerkiness for the patient, the substantial reduction in parasitic moments resulted in an overall higher-quality wrench application. Furthermore, an analysis of the residual force F_z, although not directly relevant to the rehabilitation task, revealed significantly lower values in the 4-cable configuration (Fig. 5.14). Specifically, the mean residual force in the 4-cable system was approximately $5N$, with a standard deviation of $4N$, whereas the 8-cable system exhibited a much higher residual force, with a mean of $30N$ and a standard deviation of $12N$. However, it is important to note that in the 4-cable configuration, the pulleys were placed at pelvic height, resulting in a predominantly planar setup. This inherently aligns well with the primarily planar nature of the rehabilitation task, potentially explaining the observed reduction in residual forces. In contrast, the 8-cable system, which features pulleys distributed across multiple height levels, introduces a greater degree of force coupling in the vertical direction, leading to higher residual forces in F_z. Consequently, the comparison regarding residual force reduction may be biased by the geometric configuration of the

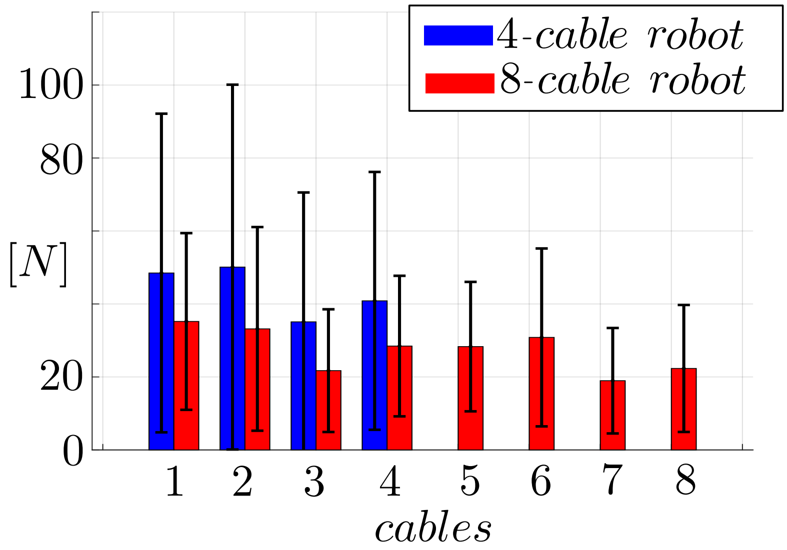

Figure 5.12: Tensions on each cable (experimental).

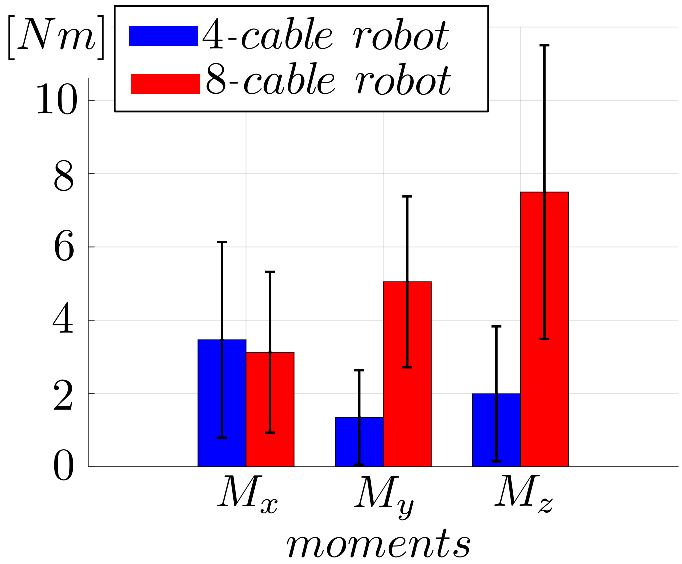

Figure 5.13: Parasitic moments (experimental).

systems, rather than solely by the number of cables.

To further validate the accuracy of the framework, the simulated Maximum Parasitics Index (MPI) and Maximum Tension Index (MTI) were extracted from colormaps (Fig. 5.8, 5.9) at the positions corresponding to the real trajectory. The MPI and MTI were then recomputed using experimental data over the full trajectory. The results (Fig. 5.15,5.16) indicate that, for the 8-cable robot, the real MPI and MTI closely align with the predicted values. Regarding the 4-cable robot, MPI was slightly overestimated, while MTI was a little underestimated. Overall, the findings validate the framework's effectiveness in both relative performance comparisons, such as evaluating trade-offs between 4-cable and 8-cable systems, and absolute performance estimation. The framework provides consistent numerical predictions of system performance in terms of cable tensions and parasitic wrench for a given task.

These findings strongly support the feasibility of replacing an 8-cable CDWA with a more accessible, cost-effective, and simpler 4-cable system while even achieving im-

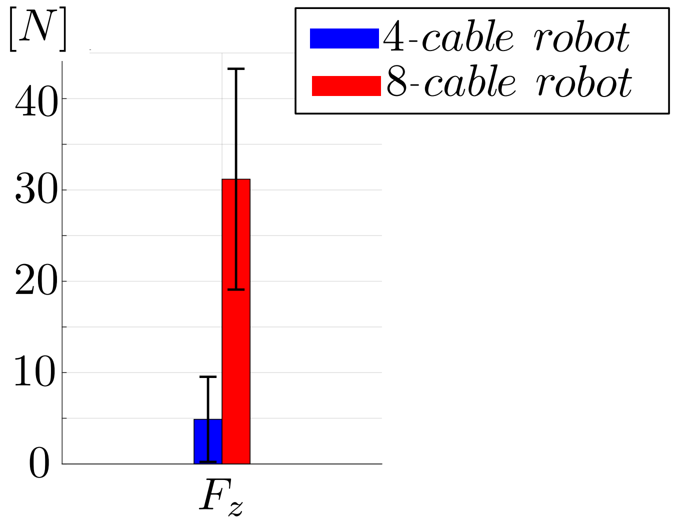

Figure 5.14: Residual force (experimental).

proved performance in terms of parasitic wrench minimization. The experimental validation confirms that the proposed analysis and optimization framework is a reliable tool for assessing and optimizing the performance of cable-driven rehabilitation devices.

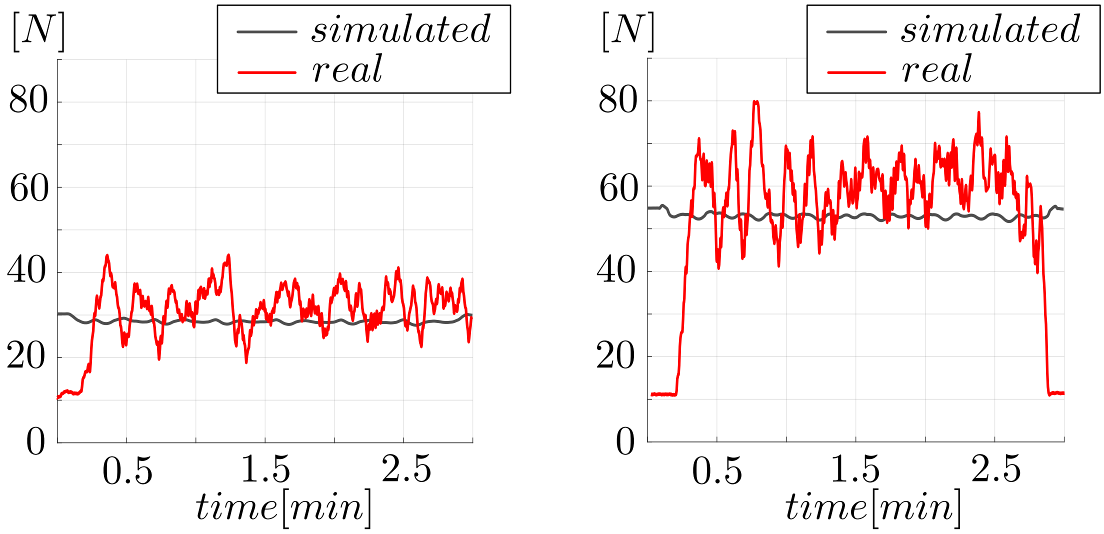

(a) MTI 8-Cable robot (RobUST)

(b) MTI 4-cable robot

Figure 5.15: Comparison of simulated and measured MTI values over six laps of the experiment. The black lines represent the average simulated MTI values, while the red lines indicate the instantaneous values of the real MTIs.

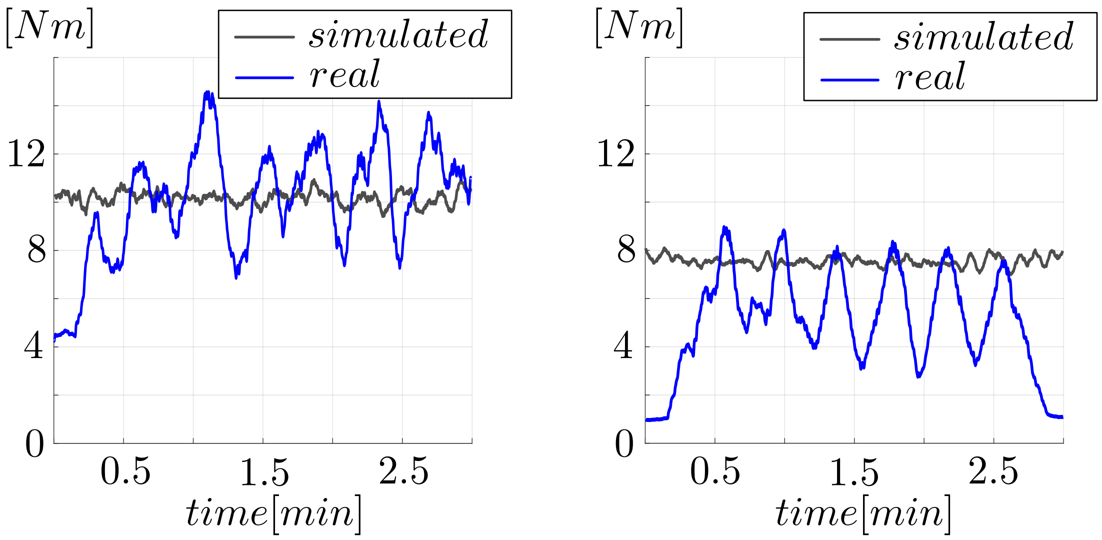

(a) MPI 8-Cable robot (RobUST)

(b) MPI 4-cable robot

Figure 5.16: Comparison of simulated and measured MPI values over six laps of the experiment. The black lines represent the average simulated MPI values, while the red lines indicate the instantaneous values of the real MPIs.

Chapter 6

Conclusions

Cable-Driven Wrench Applicators (CDWAs), a specialized subset of Cable-Driven Parallel Robots (CDPRs), are widely employed in robotics for the precise application of forces and moments at the end-effector through cable actuation. However, to the best of the author's knowledge, existing literature lacks a comprehensive framework for evaluating and optimizing these systems when used specifically for wrench application. As the demand for such systems continues to grow across various applications, a structured methodology was needed to address key challenges, including: (i) the variability in control strategies depending on the number of employed cables, (ii) the management of undesired wrench components that naturally arise when a subset of wrench components is controlled, (iii) ensuring that cable tensions remain positive and bounded while satisfying pose-dependent force requirements, and (iv) developing meaningful performance metrics for wrench application.

This thesis started to address this gap by introducing an analytical framework designed to systematically analyze and compare CDWAs, regardless of the number of cables or the specific task being performed. The proposed methodology was developed in three main stages. First, in Chapter 3, a tension computation strategy was introduced, under the assumption that the number of cables exceeds the number of controlled wrench components. Next, in Chapter 4, three performance metrics were proposed to quantify CDWA efficiency: the *Overall Performance Index* (OPI) for selecting the optimal tension distribution strategy, and the *Maximum Tension Index* (MTI) and *Maximum Parasitic-Wrench Index* (MPI) for assessing cable tensions and undesired wrench components. Finally, in Chapter 5, the framework was applied to simulate and evaluate the feasibility of replacing an 8-cable with a 4-cable robot for a rehabilitation task.

Results showed that a 4-cable system performs as well as an 8-cable system in applying a given force along a given trajectory, while maintaining applied moments under control. Cable tensions, however, are comparatively higher in the 4-cable system, despite tension minimization being applied during the tension computation. Overall, results validated the feasibility of performing the rehabilitation task using the simplified 4-cable design. These insights were confirmed by a real-world experiment, further reinforcing the effectiveness of the proposed evaluation methodology.

Beyond the specific case of the 4-cable and 8-cable systems analyzed, this study highlights the broader applicability of the proposed framework. The developed methodology can be extended to evaluate and compare other cable-driven robotic systems, providing valuable insights for optimizing CDWA designs in various application domains. Future research may further refine these performance metrics, explore alternative optimization strategies for tension distribution, and assess the framework's applicability in non-rehabilitation contexts.

Appendices

Appendix A

General Formulation of KKT Conditions

The general formulation of the Karush-Kuhn-Tucker (KKT) conditions is given in [33] and is briefly recalled here.

Considering the following constrained optimization problem:

$$\min_{x} f(x) \tag{A.1}$$

subject to

$$g_i(x) \leq 0, \quad i = 1, \ldots, m, \tag{A.2}$$
$$h_j(x) = 0, \quad j = 1, \ldots, p, \tag{A.3}$$

where:

- $f(x)$ is the objective function,
- $g_i(x)$ are the inequality constraints,
- $h_j(x)$ are the equality constraints.

The *Lagrangian* function for this problem is:

$$\mathscr{L}(x, \boldsymbol{\mu}, \boldsymbol{\nu}) = f(x) + \sum_{i=1}^{m} \mu_i g_i(x) + \sum_{j=1}^{p} \nu_j h_j(x), \tag{A.4}$$

where:

- μ_i are the Lagrange multipliers for the inequality constraints $g_i(x)$,
- ν_j are the Lagrange multipliers for the equality constraints $h_j(x)$.

For a feasible solution x^* to be optimal, it must satisfy the *Karush-Kuhn-Tucker (KKT) conditions*:

- 1. Stationarity

$$\nabla_x \mathscr{L}(x, \boldsymbol{\mu}, \boldsymbol{\nu}) = \nabla f(x) + \sum_{i=1}^{m} \mu_i \nabla g_i(x) + \sum_{j=1}^{p} \nu_j \nabla h_j(x) = 0. \tag{A.5}$$

- 2. Primal Feasibility

$$g_i(x) \leq 0, \quad \forall i, \tag{A.6}$$
$$h_j(x) = 0, \quad \forall j. \tag{A.7}$$

- 3. Dual Feasibility

$$\mu_i \geq 0, \quad \forall i. \tag{A.8}$$

- 4. Complementary Slackness

$$\mu_i g_i(x) = 0, \quad \forall i. \tag{A.9}$$

Interpretation of KKT conditions and role in optimality

The *stationarity condition* (A.5) ensures that the gradient of the Lagrangian with respect to the decision variables x is zero. At an optimal point, the objective function cannot be further minimized without violating at least one constraint.

The *Primal Feasibility Condition* (A.7) ensures that the solution x^* satisfies all given constraints of the problem, i.e., it remains within the feasible region defined by the inequality and equality constraints.

The *Dual Feasibility Condition* (A.8) guarantees that Lagrange multipliers μ_i associated with the inequality constraints must be non-negative. The sign of μ_i determines the influence of the constraint on the solution. A negative μ_i would indicate that the constraint is pushing the solution in the wrong direction, which contradicts optimality. Non-negative multipliers ensure that constraints are correctly contributing to the minimization process.

The *Complementary Slackness Condition* (A.9) enforces that either:

- The constraint is active ($g_i(x) = 0$), meaning it is exactly satisfied at the optimal solution, or
- The corresponding Lagrange multiplier is zero ($\mu_i = 0$), indicating that the constraint is inactive and does not affect the solution.

This condition prevents unnecessary constraints from distorting the solution. Only the active constraints influence the optimality conditions, while inactive constraints (those not affecting the solution) have zero multipliers.

Together, the KKT conditions ensure that:

- The solution is a critical point of the Lagrangian (*stationarity*), ensuring a balance between the objective function and the constraints.
- The solution satisfies all problem constraints (*primal feasibility*).
- The Lagrange multipliers for inequality constraints are non-negative (*dual feasibility*), ensuring that constraints influence the solution in the correct direction.

- Only the active constraints influence the optimal solution (*complementary slackness*), preventing unnecessary constraints from affecting the outcome.

These conditions are necessary for optimality in constrained optimization problems. In cases where the problem satisfies convexity conditions, the KKT conditions are also sufficient for global optimality.

List of Figures

Bibliography

[1] Y. Mao and S. K. Agrawal, “Design of a cable-driven arm exoskeleton (carex) for neural rehabilitation,” *IEEE Transactions on Robotics*, vol. 28, 2012.

[2] J. V. Zitzewitz, G. Rauter, R. Steiner, A. Brunschweiler, and R. Riener, “A versatile wire robot concept as a haptic interface for sport simulation,” in *IEEE International Conference on Robotics and Automation, ICRA 2009*, 2009.

[3] H. Saafi, M. A. Laribi, and S. Zeghloul, “Force control implementation of a haptic device for a medical use,” in *Robotics and Mechatronics*, vol. 37, pp. 143–151, 2016.

[4] M. Shoaib, E. Asadi, J. Cheong, and A. Bab-Hadiashar, “Cable driven rehabilitation robots: Comparison of applications and control strategies,” *IEEE Access*, vol. 9, 2021.

[5] A. Pott, *Cable-driven parallel robots.* Springer, 2013.

[6] H. Xiong and X. Diao, “A review of cable-driven rehabilitation devices,” *Disability and Rehabilitation: Assistive Technology*, vol. 15, no. 8, pp. 885–897, 2020.

[7] Y. Mao and S. K. Agrawal, “Design of a cable-driven arm exoskeleton (carex) for neural rehabilitation,” *IEEE Transactions on Robotics*, vol. 28, no. 4, pp. 922–931, 2012.

[8] A. S. Santamaria V, Ai X, “A motor learning-based postural intervention with a robotic trunk support trainer to improve functional sitting in spinal cord injury: case report,” *Spinal Cord Ser Cases*, 2022.

[9] L. T. . A. S. Santamaria, V., “Feasibility and tolerance of a robotic postural training to improve standing in a person with ambulatory spinal cord injury,” *Spinal Cord Ser Cases 7, 94*, 2021.

[10] L. S. J. A. S. Stramel, D.M.; Winterbottom, “Overground robotic gait trainer mtpad improves gait symmetry and weight bearing in stroke survivors,” *Bioengineering*, vol. 10, p. 698, 2023.

[11] A. S. Santamaria V, Ai X, “A motor learning-based postural intervention with a robotic trunk support trainer to improve functional sitting in spinal cord injury: case report,” *Spinal Cord Ser Cases*, 2022.

[12] L. T. K. M. e. a. Santamaria, V., “The robotic trunk-support-trainer (trust) to measure and increase postural workspace during sitting in people with spinal cord injury,” *Spinal Cord Ser Cases 6, 1*, 2020.

[13] E. Idà and M. Carricato, "Static workspace computation for underactuated cable-driven parallel robots," *Mechanism and Machine Theory*, vol. 193, 2024.

[14] E. Idà and M. Carricato, "A new performance index for underactuated cable-driven parallel robots," in *Mechanisms and Machine Science*, vol. 104, 2021.

[15] C. Gosselin and M. Grenier, "On the determination of the force distribution in overconstrained cable-driven parallel mechanisms," *Meccanica*, vol. 46, 2011.

[16] K. Shi, A. Song, Y. Li, H. Li, D. Chen, and L. Zhu, "A cable-driven three-dof wrist rehabilitation exoskeleton with improved performance," *Frontiers in Neurorobotics*, vol. 15, 2021.

[17] V. Mattioni, E. Idà, and M. Carricato, "Force-distribution sensitivity to cable-tension errors in overconstrained cable-driven parallel robots," *Mechanism and Machine Theory*, vol. 175, p. 104940, 2022.

[18] M. Hassan and A. Khajepour, "Minimization of bounded cable tensions in cable-based parallel manipulators," in *2007 ASME International Design Engineering Technical Conferences and Computers and Information in Engineering Conference, DETC2007*, vol. 8 PART B, 2008.

[19] G. Boschetti and A. Trevisani, "Cable robot performance evaluation by wrench exertion capability," *Robotics*, vol. 7, 2018.

[20] I. Bonev and C. Gosselin, "Analytical determination of the workspace of symmetrical spherical parallel mechanisms," *IEEE Transactions on Robotics*, vol. 22, no. 5, pp. 1011–1017, 2006.

[21] M. Carricato and J.-P. Merlet, "Direct geometrico-static problem of underconstrained cable-driven parallel robots with three cables," vol. 5, pp. 3011–3017, 05 2011.

[22] A. Pott and V. Schmidt, "On the forward kinematics of cable-driven parallel robots," in *2015 IEEE/RSJ International Conference on Intelligent Robots and Systems (IROS)*, pp. 3182–3187, 2015.

[23] X. Garant, A. Campeau-Lecours, P. Cardou, and C. Gosselin, "Improving the forward kinematics of cable-driven parallel robots through cable angle sensors," in *Cable-Driven Parallel Robots* (C. Gosselin, P. Cardou, T. Bruckmann, and A. Pott, eds.), (Cham), pp. 167–179, Springer International Publishing, 2018.

[24] F. Ennaiem, A. Chaker, J. Sandoval, S. Bennour, A. Mlika, L. Romdhane, S. Zeghloul, and M. A. Laribi, "Cable-driven parallel robot accuracy improving using visual servoing," in *Advances in Service and Industrial Robotics* (A. Müller and M. Brandstötter, eds.), (Cham), pp. 97–105, Springer International Publishing, 2022.

[25] D. M. Stramel and S. K. Agrawal, "Validation of a forward kinematics based controller for a mobile tethered pelvic assist device to augment pelvic forces during walking," in *2020 IEEE International Conference on Robotics and Automation (ICRA)*, pp. 10133–10139, 2020.

[26] S. K. Mustafa and S. K. Agrawal, "On the force-closure analysis of n-dof cable-driven open chains based on reciprocal screw theory," *IEEE Transactions on Robotics*, vol. 28, no. 1, pp. 22–31, 2012.

[27] M. Gouttefarde, J. Lamaury, C. Reichert, and T. Bruckmann, "A versatile tension distribution algorithm for n -dof parallel robots driven by $n+2$ cables," *IEEE Transactions on Robotics*, vol. 31, no. 6, pp. 1444–1457, 2015.

[28] X. Jin, X. Cui, and S. K. Agrawal, "Design of a cable-driven active leg exoskeleton (c-alex) and gait training experiments with human subjects," in *IEEE International Conference on Robotics and Automation ICRA 2015*, vol. 2015-June, 2015.

[29] W. Kraus, A. Spiller, and A. Pott, "Energy efficiency of cable-driven parallel robots," in *2016 IEEE International Conference on Robotics and Automation (ICRA)*, pp. 894–901, 2016.

[30] Y. Zou, X. Wu, B. Zhang, Q. Zhang, A. Zhang, and T. Qin, "Stiffness analysis of parallel cable-driven upper limb rehabilitation robot," *Micromachines*, vol. 13, p. 253, 02 2022.

[31] A. González-Rodríguez, A. Martín-Parra, S. Juárez-Pérez, D. Rodríguez-Rosa, F. Moya-Fernández, F. J. Castillo-García, and J. Rosado-Linares, "Dynamic model of a novel planar cable driven parallel robot with a single cable loop," *Actuators*, vol. 12, no. 5, 2023.

[32] A. Pott, *On the Limitations on the Lower and Upper Tensions for Cable-Driven Parallel Robots*, pp. 243–251. 05 2014.

[33] B. Ghojogh, A. Ghodsi, F. Karray, and M. Crowley, "Kkt conditions, first-order and second-order optimization, and distributed optimization: Tutorial and survey," 2021.

[34] M. I. Khan, V. Santamaria, J. Kang, B. M. Bradley, J. P. Dutkowsky, A. M. Gordon, and S. K. Agrawal, "Enhancing seated stability using trunk support trainer (trust)," *IEEE Robotics and Automation Letters*, vol. 2, no. 3, pp. 1609–1616, 2017.

[35] P. Gribble, "The star excursion balance test as a measurement tool.," *Athletic Therapy Today*, vol. 8, no. 2, 2003.

[36] S. K. Banala, S. K. Agrawal, S. H. Kim, and J. P. Scholz, "Novel gait adaptation and neuromotor training results using an active leg exoskeleton," *IEEE/ASME Transactions on Mechatronics*, vol. 15, no. 2, pp. 216–225, 2010.

[37] M. Khan, T. Luna, V. Santamaria, I. Omofuma, D. Martelli, E. Rejc, J. Stein, S. Harkema, and S. Agrawal, "Stand trainer with applied forces at the pelvis and trunk: Response to perturbations and assist-as-needed support," *IEEE transactions on neural systems and rehabilitation engineering IEEE Engineering in Medicine and Biology Society*, vol. 27, 2019.

[38] J. Pierrepont, L. Walter, B. Miles, E. Marel, J. Baré, M. Solomon, S. McMahon, and A. Shimmin, "Pelvic tilt in the standing, supine and seated positions," *Orthopaedic Proceedings*, vol. 98-B, 2016.